

Review

A review on powder-based additive manufacturing for tissue engineering: selective laser sintering and inkjet 3D printing

Seyed Farid Seyed Shirazi^{1,2}, Samira Gharehkhani¹, Mehdi Mehrali^{1,2},
Hooman Yarmand¹, Hendrik Simon Cornelis Metselaar¹,
Nahrizul Adib Kadri² and Noor Azuan Abu Osman²

¹Department of Mechanical Engineering and Advanced Material Research Center, University of Malaya, 50603 Kuala Lumpur, Malaysia

²Department of Biomedical Engineering, Faculty of Engineering, University of Malaya, 50603 Kuala Lumpur, Malaysia

E-mail: faridseyedshirazy@yahoo.co.uk and m.mehrli@siswa.um.edu.my

Received 10 December 2014, revised 16 March 2015

Accepted for publication 16 March 2015

Published 5 May 2015



CrossMark

Abstract


Since most starting materials for tissue engineering are in powder form, using powder-based additive manufacturing methods is attractive and practical. The principal point of employing additive manufacturing (AM) systems is to fabricate parts with arbitrary geometrical complexity with relatively minimal tooling cost and time. Selective laser sintering (SLS) and inkjet 3D printing (3DP) are two powerful and versatile AM techniques which are applicable to powder-based material systems. Hence, the latest state of knowledge available on the use of AM powder-based techniques in tissue engineering and their effect on mechanical and biological properties of fabricated tissues and scaffolds must be updated. Determining the effective setup of parameters, developing improved biocompatible/bioactive materials, and improving the mechanical/biological properties of laser sintered and 3D printed tissues are the three main concerns which have been investigated in this article.

Keywords: additive manufacturing, inkjet 3D printing, selective laser sintering, biomaterials, tissue engineering

1. Introduction

Additive manufacturing (AM) is a technique for fabricating parts in precise geometry using computer aided design (CAD) and computer aided manufacturing (CAM) [1]. In each AM technique, the 3D model designed in CAD software is

converted to STL format, which is a triangular mesh of the object, and then the STL format is sliced into 2D profile layers. Each sliced layer of the model is bonded to the previous layer on the build platform until a 3D part is fabricated. The principal AM technologies are selective laser sintering (SLS), stereolithography (SLA), fused deposition modeling (FDM), direct metal laser sintering (DMLS), and inkjet 3D printing (3DP) techniques [2, 3]. Depending on the process and materials used, each technique has both strong and weak points. The most significant elements that should be considered in choosing an appropriate AM technology for a

 Content from this work may be used under the terms of the [Creative Commons Attribution 3.0 licence](https://creativecommons.org/licenses/by/3.0/). Any further distribution of this work must maintain attribution to the author(s) and the title of the work, journal citation and DOI.

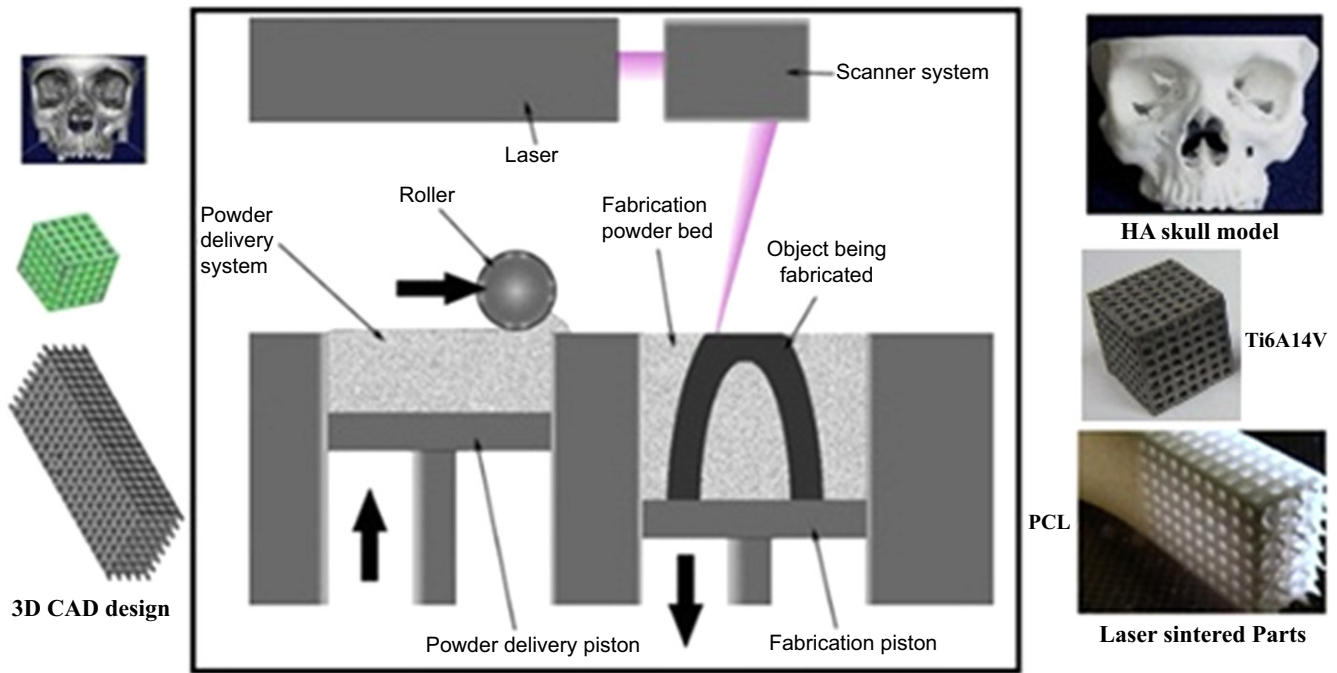


Figure 1. Schematic of SLS from 3D CAD design to the laser sintering process. Reprinted from D N Silva 2008 *J. Cranio-Maxillofacial Surg.* 36 443–9, Copyright 2008, with permission from Elsevier; S Eshraghi and S Das 2010 *Acta Biomater.* 6 2467–76, Copyright 2010, with permission from Elsevier; and E Sallica-Leva *et al* 2013 *J. Mech. Behav. Biomed. Mater.* 26 98–108, Copyright 2013, with permission from Elsevier.

particular purpose are accuracy, time, and cost of fabrication. The parameter of accuracy refers to the thickness of the layers and the system of consolidation, and since AM techniques are tool-free fabrication methods, time of production can outweigh increased fabrication costs per item [3, 4].

Biomedical applications, e.g., tissues, scaffolds, and fixation devices, have specific aspects of fabrication which should be considered. For biomedical applications, the use of these AM methods without rigid support structures is strongly recommended [5]. In supportless AM methods the imprinted powders surround and support complex parts during the printing process, and after finishing the process, users can reuse all uncured support powders. Other additive processes require the building of solid support structures to support complex geometries during the printing process. Users have to discard these support structures after use, and the wasted material contributes significantly to the cost of additive technologies. In addition, removing attached supports from fabricated parts limits the ability to stack or nest parts [6].

AM approaches, particularly 3DP and SLS, are simple and adaptable to using a broad range of powders to produce porous ceramics, polymers, and metal-based tissues [7, 8]. To enhance bone regeneration in fabricated tissues, using powder-based AM techniques is recommended. These kinds of fabricated scaffolds can be filled with a porous spacer, allowing the ingrowth of a blood vessel [9].

In this article, the working principle of SLS and inkjet 3DP and modifications of these methods are reviewed. Materials used in SLS and inkjet 3DP and optimization of the effective parameters of these two powder-based AM

techniques for the fabrication of useful bone tissues and scaffolds are highlighted. Biological tests (*in vitro*, *in vivo* and apatite layer formation) conducted on the fabricated tissues and scaffolds are presented and discussed, as well as clinical works regarding fabricated objects.

2. Laser sintering technology

The SLS technique as depicted in figure 1 uses a CO₂ or Nd:YAG laser beam for scanning successive layers of powdered materials to create a 3D object [10]. Based on slicing of the digital design, the scanning patterns of each layer are computed automatically [11]. As is illustrated in figure 1, fabrication of the final parts using the SLS method includes two steps: 3D CAD design of the concept and transfer of the CAD data to the SLS machine to carry out fabrication with the desired powders.

Each AM system has a unique binding mechanism to bind the layers. The binding mechanism of SLS technology can be classified into three main categories [13, 15].

- Solid-state sintering, which is a thermal process. The binding mechanism in this category occurs between $T_m/2$ and T_m , wherein lies the melting temperature of the material in question.
- Liquid phase assisted sintering, which is commonly used for materials that are difficult to sinter. Liquid phase assisted sintering is the process of adding an additive to the powder which will melt before the matrix phase. This method is widely employed for fabrication of 3D parts

Table 1. Effect of layer thickness on average pore width and proportion of pores of a suitable size in SLS [20].

Laser power (W)	0.15 mm thickness of each layer			0.17 mm thickness of each layer			0.19 mm thickness of each layer		
	Average pore width (μm)	Range pore width (μm)	Porosity (%)	Average pore width (μm)	Range pore width (μm)	Porosity (%)	Average pore width (μm)	Range pore width (μm)	Porosity (%)
3.2	61	10–318	19	75	10–382	28	80	10–500	29
5.5	66	10–462	21	78	10–409	30	83	10–364	32
7.7	64	10–464	22	77	10–382	31	80	10–473	33
10	67	10–391	21	77	10–482	31	80	10–482	32

from ceramic materials with incorporation of a small amount of polymers which will gradually decompose and completely disappear [16].

- Full melting, which is used for metallic and ceramic materials more than polymers. In this mechanism, near full density is reached in one step by melting the powders completely by laser beam, thus avoiding lengthy post-processing steps.

In the SLS method, material properties and process factors such as laser energy density, part bed temperature, layer thickness, and hatch distance affect the structural and mechanical properties of fabricated parts [17, 18].

In this AM technique particle sizes in the range of 10–150 μm are preferred [19]. The ideal laser energy density follows from the melting point of the binders (in the liquid phase sintering method) or powders (in the full melting technique) and can be set by adjusting the laser power and scan speed [20].

By decreasing the laser scanning speed, denser parts may be obtained. This is caused by the longer interaction time between the powder and the laser beam, which boosts the rate of energy delivered to the powder bed [21]. A higher laser scan speed results in less energy transferred to the materials [22], leading to less sintering and in turn to more porosity. It should be noted that this case occurs especially in low melting point systems. Increasing the energy delivered to the powder bed promotes better melting of the powders, enabling more liquid phase to flow and infiltrate into the voids between the particles, which can lead to a denser structure [21].

On the other hand, sufficiently high energy density leads to the complete melting of the binder, which reduces material delamination and increases the density of the fabricated parts. Although the higher energy density increases the mechanical properties of the final parts, it sometimes leads to inaccurate dimensions [17]. As a practical matter, because the time of exposure of the material to the laser beam is too short, fabricating high-density parts is difficult. It is reported that an isothermal process as a second step using a furnace with a lower temperature than that obtained under the laser beam improves the density of the final parts [23].

Tan *et al* [24] have also conducted some preliminary laser sintering tests to determine the range of suitable processing parameters used in the SLS system. In their study, only one layer of material with 0.1 mm thickness was sintered

to determine the parameter setting. First, they set the bed temperature to 110 °C and reported the formation of necks between particles at a laser energy of 12 W; however, there was delamination between the specimen layers. To improve the quality of the specimens, a higher bed temperature was used. In this study the optimum SLS processing factors were found to be 140 °C for the bed temperature and 12 W for the laser energy. For the materials with lower density and lower melting point, the applied laser power was lower [19, 25, 26].

The effect of layer thickness on the open porosity of parts fabricated by SLS has been studied by Salvani *et al* [20]. The results demonstrated that layer thickness has the greatest impact on the average pore width and on the proportion of pores with a proper size to facilitate bone regeneration. This phenomenon can be caused by thicker powder layers allowing less fusion between particles, resulting in less densification and higher open porosity. Table 1 summarizes the effect of layer thickness on the average pore size of fabricated SLS samples.

Similar results for the influence of layer thickness on the porosity and layer bonding have been obtained in other studies [21]. It was concluded that smaller layer thickness leads to stronger bonding between the layers and decreases the porosity of the parts. Finding an optimum layer thickness is necessary depending on which application is desired. The minimum layer thickness that can be used effectively is determined by the maximum particle size of the powder. If a too-small layer thickness is chosen, the blade will drag non-melted large particles or chunks of melted particles, displacing the previous sintered layers from their position. Consequently, layer thickness for denser product must be set to the minimum layer thickness and vice versa [21].

Hatch distance is another important parameter with respect to the properties of the parts fabricated by SLS. It has been confirmed that with a large increase in hatch distance in the prototype, there are dramatic changes in pore channels in its structure [27]. The different microstructure resulting from a large hatch distance can be explained by the overlapping theory. Overlapping addresses to what degree a new laser line scans over the previously scanned track. Decreasing the hatch distance brings the scan lines closer to one another until they overlap. As an example, if the laser beam spot size is 0.4 mm, the parts processed with a hatch distance less than the laser spot size (e.g., 0.1, 0.2, and 0.3 mm) have different degrees of

overlap. A large part of the laser spot may scan over a previously scanned line and accordingly increase the flowing and spreading of the liquid between adjacent scan lines, which leads to an enhancement of the inter-line bonding and a reduction in porosity. When a hatch distance of 0.4 mm is chosen, no overlapping is observed, resulting in appropriate connectivity of the matrix and a more porous part [28].

Another phenomenon which can affect the surface morphology of samples fabricated by SLS is balling [29, 30]. Balling is defined as an agglomeration of the particles, occurring where the liquid phase breaks up into a row of spheres to reduce surface energy. The main factor leading to balling is the Gibbs–Marangoni effect, which is the mass transfer along an interface between two fluids due to the surface tension gradient [31]. In terms of temperature association, this phenomenon is also called thermo-capillary convection. Balling has a direct effect on creating large pores but is not a definitive solution for fabricating tissues with desired pores. Early experiments in using the SLS method for the fabrication of metallic parts confirmed balling during the process [32]. To diminish the balling effect and consequently to have a uniformly sintered specimen, not only do the SLS parameters need to be set, but multiphase powders need to be designed by mixing different materials with various melting temperatures or by employing a pre-alloyed powder system in which melting takes place over a temperature range [33, 34].

2.1. Commonly used materials in SLS

2.1.1. Polymers. Two types of thermoplastics are used in SLS: semi-crystalline and amorphous [35]. An amorphous material has chain molecules arranged in a random manner, and semi-crystalline material has chain molecules arranged in an orderly structure. Semi-crystalline and amorphous materials have different thermal properties which determine the fabrication parameters in SLS.

The most important characteristics that determine the application of thermoplastic polymers are the glass transition temperature, T_g , and the melting temperature, T_m . The glass transition temperature T_g is the temperature where a rapid decrease in E (elastic modulus) occurs. It can be observed in amorphous material. Melting does not occur until the polymer reaches a higher temperature, T_m . Below T_g , the polymer is in the glass state and the molecular motion along the chain is frozen. When the temperature rises from T_g to approximately ($T_g + 30$ K), the molecular motion increases, causing the modulus to drop. Just above T_g , the polymer behaves like a highly viscous liquid in which the chains are all tangled up with their neighbors [36, 37].

It has been also reported that a majority of semi-crystalline polymers have a glass transition temperature (T_g) below or close to room temperature (-100 to 50 °C) and a melting temperature (T_m) above 100 °C (between 100 and 400 °C) at which a considerable volume change occurs. On the other hand, amorphous polymers do not have a characteristic melting temperature range [38]. They have a T_g of ~ 100 °C, above which the material will progressively evolve to a leathery, rubbery, and finally liquid state as the

temperature increases, with no obvious transitions [38–40]. It is important to mention that both T_g and T_m depend directly on molecular weight. This is why a different setup is needed to run an SLS system for different thermoplastic materials.

As mentioned, the power of the laser applied in an SLS system has an important effect on the mechanical properties of the fabricated models. For a semi-crystalline polymer powder, laser consolidation occurs by heating it to above its T_m since semi-crystalline powders have a molecular structure with spiky melt points. They do not gradually become softer with a temperature increase and remain hard until a given quantity of heat is absorbed and then quickly change into a viscous liquid. Shrinkage often happens simultaneously with freezing. To minimize this drawback, it is better to preheat the powders and to keep them in a furnace below their melting temperature for several hours [38].

Consolidation of amorphous polymer powder happens by laser heating over T_g , at which point the polymer is in a much more viscous position than semi-crystalline polymers at a similar temperature [41]. Unlike semi-crystalline polymers, amorphous polymers do not have a spiky melt point and soften slowly as the temperature rises. The viscosity of these materials changes when heated, but they seldom are as easy flowing as semi-crystalline materials.

There are a number of studies on using natural and synthesized polymers in SLS. For example, cellulose, the most abundant natural polymer [42], has been used to fabricate SLS scaffolds [18]. An important synthetic biodegradable polymer material is polycaprolactone (PCL) This material is semi-crystalline with high thermal stability and a degradation period of approximately two years [43]. Due to the good biocompatibility, bioresorbability, and processability of PCL, this polymer is used for tissue engineering [25] and cartilage repair [44–46].

2.1.2. Ceramics. SLS of ceramic materials can be either direct or indirect. Direct SLS of ceramics can be powder based or slurry based. In the powder-based method, the packing density of the powder layers is low, leading to a lower sintered density and also leading to cracks due to thermal stresses in the parts [47]. Efforts have been made to develop direct SLS to produce fully dense ceramic composites [48]. In this method high laser energy is applied to a preheated powder bed, causing the powder to melt and avoiding thermal stress cracking.

On the other hand, slurry-based direct SLS takes advantage of more homogeneous and much more densely packed powder layers obtained from the slurry process. The concern is that this method produces parts with lower strength due to thermal cracks and microstructural inhomogeneities [49, 50].

Agglomeration of powders is a concern with using slurry-based SLS. An effective way to avoid agglomeration during laser sintering may be to process at a lower scanning speed or to employ a surfactant in a very low concentration [51]. Using a surfactant helps obtain a homogeneous green part which can demonstrate better mechanical properties. This

method is appropriate when the purpose is the fabrication of ceramic scaffolds with bioactive ceramics such as calcium silicate and hydroxyapatite. Calcium silicate (CS, CaSiO_3) is a bioactive ceramic that has been explored for tissue engineering applications over the last two decades [52–55]. Many studies have shown that CS is able to form an apatite layer on its surface by soaking in simulated body fluid (SBF) [55]. CS scaffolds with an interconnected pore structure can be made by SLS [56]. Another commonly used ceramic in tissue engineering and the SLS method is hydroxyapatite (HA, $\text{Ca}_{10}(\text{PO}_4)_6(\text{OH})_2$). HA is a calcium phosphate ceramic (CP) material that is biocompatible and bioactive due to its similarity to the mineral constituents of human bone and teeth [57, 58]. Nanosized HA powder has a high specific surface area which can improve the sinterability and densification of scaffolds. Although pure CS and HA are known as biocompatible materials, the poor mechanical properties of fabricated scaffolds have limited their application [53, 58].

The indirect method uses polymers as a binder with ceramic powders as the main matrix and involves the melting of sacrificial organic polymer to obtain a green part. The green parts are subsequently sintered to produce the final porous ceramic parts [59]. Even though the materials used in this method include both polymer and ceramic as starting materials, the final part is pure ceramic and not a composite.

It has been confirmed that semi-crystalline polymers are preferred over amorphous polymers for use as the binder phase due to their higher density compared with amorphous polymers [59]. However, semi-crystalline shrinks by 4–5 vol% upon solidification, causing component distortion. To reduce distortion, all material is preheated to just below T_m with SLS heating it in just a small window, i.e., the temperature window between the onset of polymer melting during heating and crystallization during cooling [59, 60]. After SLS the part must be cooled to room temperature slowly.

Fabrication of scaffolds from bioactive glass materials using the indirect method has been reported. Bioactive glass materials with different compositions, e.g., 45S5, 58S, and 13–93, can be used as scaffold materials [17, 61, 62]. Bioactive glass materials have numerous advantages over other bioactive ceramics like sintered hydroxyapatite. For example, it has been shown that dissolution products from bioactive glasses upregulate the expression of genes that control osteogenesis [63], which explains the high rate of bone formation [64, 65].

2.1.3. Metals. Because metals possess excellent compressive strengths and also high fatigue resistance, porous metallic scaffolds such as titanium (Ti) and tantalum (Ta) and biocompatible alloys such as CoCr and nitinol have been proposed as bone replacement materials, but unlike bioactive ceramics or biocompatible polymeric scaffolds, biomolecules cannot be integrated into metallic scaffolds. The lack of degradability of metallic implants restricts the use of these kinds of scaffolds. The main concern with embedding metallic scaffolds is metal ion release into body fluid,

leading to sarcoma. Coating the surface of metallic scaffolds with bioactive ceramics such as HA or CS or using surface finishing methods is highly recommended to improve the biological properties of metallic scaffolds [66].

One category of SLS is selective laser melting (SLM), in which very high laser energy is applied to fully melt metals into a solid homogeneous mass. Different CoCrMo alloys meeting the requirements for tissue applications have been investigated to observe the effect of the laser melting process on corrosion and metal release in biologically relevant fluids [67]. The strong temperature gradient as well as the rapid cooling during the laser melting process induces the formation of a fine cellular microstructure with molybdenum (Mo) enriched at the grain boundaries and suppresses the formation of large micron-sized carbides, resulting in higher corrosion resistance compared with cast alloy.

Dental implants have been fabricated from stainless steel and Ti6Al4V and CrCo alloys by the SLM method [11]. For the consolidation of the powders, two different binding mechanisms are used, depending on the materials and alloys. The first mechanism is liquid phase sintering, where a polymer is liquefied by a laser beam with an energy density of 1 J mm^{-3} and acts as a binder for the stainless steel particles. This technique needs an additional heating cycle in which the polymer is burned out and the green part is further sintered and infiltrated with, e.g., bronze to reach a high density. The second technique is used for Ti6Al4V or CoCr alloy and consists of melting the metal powder completely by a laser beam with an energy density of 200 J mm^{-3} , avoiding the need for post-processing. Further surface modification of the laser-melted Ti6Al4V alloy has shown improvement in biocompatibility and a reduction in post-implant complications [68]. The alloys fabricated by SLM are functionalized with a pharmaceutically relevant biomolecule (paracetamol) using phosphonic acid-based self-assembled monolayers (SAMs) to be used as a biocompatible coating layer for drug and protein delivery [68].

2.1.4. Composites. Polymers are elastic and have low stiffness, whereas ceramics are rigid and brittle [69]. By mixing ceramics and polymers into composites, the mechanical properties are significantly improved because the problem of brittleness and the difficulty of shaping hard ceramics can be overcome [53, 58, 70].

Numerous studies have been done to evaluate the potential of SLS in producing composite scaffolds containing polymer and ceramic [19, 71, 72]. The main issue for ceramic/polymer composites is the agglomeration of ceramic powders into the polymer matrix. Using SLS for sintering, a mixture of ceramic and polymer powders can solve this problem due to the uniform distribution of ceramic into the matrix. Studies regarding SLS have included sintering hydroxyapatite powders coated with polymeric binders [72, 73].

A study of scaffolds consisting of microspherical calcium phosphate (CP)/poly(hydroxybutyrate-co-hydroxyvalerate) (PHBV) and carbonated hydroxyapatite (CHA)/poly(L-lactic

Table 2. Mechanical properties and setup parameters of laser-melted Ti6Al4V alloy.

Yielding strength (MPa)	Ultimate strength (MPa)	Scanning velocity (mm s ⁻¹)	Laser power (W)	Reference
990 ± 5	1095 ± 10	225	195	[85]
1110 ± 9	1267 ± 5	1600	225	[86]

acid) (PLLA) has shown an improvement in biological properties. Laser-sintered HA/polyetheretherketone (PEEK) can also satisfy the requirements of tissues and scaffolds [74]. PEEK, a synthetic polymer, is a semi-crystalline thermoplastic with excellent mechanical and chemical resistance properties, even at high temperatures. Its Young's modulus is 3.6 GPa, and its tensile strength is 90 to 100 MPa [75, 76]. PEEK has a glass transition at approximately 143 °C and melts at approximately 343 °C. Since PEEK has a much lower melting point than HA, it is possible to induce sintering of PEEK at temperatures near T_g and to bind and partially expose the HA particles within the sintered PEEK matrix.

Up to now, there have been few works regarding the fabrication of porous CS scaffolds using SLS and enhancing their mechanical properties by adding HA whiskers at the same time. In a previous study, porous scaffolds from CP materials with different weight ratios of TCP/HAP (0/100, 10/90, 30/70, 50/50, 70/30, and 100/0) were fabricated via SLS [77].

2.2. Mechanical properties of SLS parts

Depending on the material and physical properties of the final products, various mechanical properties can be obtained for fabricated scaffolds. A high compressive strength of 18.2 ± 1.2 MPa has been reported for laser sintered CS scaffolds with an interconnected pore structure [56]. Shuai *et al* [78] have reported a Vickers hardness of 4.00 ± 0.13 GPa and a fracture toughness of 1.28 ± 0.03 MPa m^{1/2} for a scaffold made from high surface area HA nano powder by using SLS with a laser energy density of 4 J mm^{-2} . Shuai *et al* [79] have fabricated scaffolds via SLS of a composite of CS and poly (vinyl alcohol) (PVA). It was reported that the scaffolds could not be fabricated successfully due to decreased fusion between PVA particles when CS was higher than 20 wt%. For scaffolds containing 15 wt% CS, the compressive strength and compressive modulus reached optimum values of 184 ± 15 kPa and 1.6 ± 0.3 MPa, respectively. Tailoring the porous structure and interconnected pore network in the scaffolds has been reported to increase strength. Feng *et al* [80] have been able to successfully fabricate a highly porous structure with a pore size of 0.5–0.8 mm and fully interconnected pore network scaffolds from HA whiskers incorporated into a CS matrix by SLS. They showed that applying SLS could enhance the compressive strength, compressive Young's modulus, and fracture toughness of CS with HA whiskers ranging from 0 to 20 wt%. Moreover, for scaffolds made with cellulose material, the specimens with lower particle size showed a higher degree of sintering, a significant level of closed pores, and greater mechanical strength [18].

An interesting work done by Gao *et al* [62] has presented the mechanical properties of SLS scaffolds made with nano-58 S bioactive glass/graphene composite. Recently graphene, a 2D single layer of sp² carbon atoms, has attracted great interest for producing the next generation of nanocomposites used in scaffold fabrication [81]. Due to its superior biocompatibility and mechanical properties, graphene can be used in small amounts as a reinforcing phase in composites. The optimum compressive strength and fracture toughness of the 58 S/graphene scaffolds reached 49 ± 3 MPa and 1.9 ± 0.1 MPa m^{1/2} with a graphene content of 0.5 wt%, indicating significant improvement of 105% and 38% respectively compared with pure 58 S.

Velez *et al* [82] have reported using of 13–93 bioactive glass with a chemical composition of 53% SiO₂, 4% P₂O₅, 20% CaO, 5% MgO, 6% Na₂O, and 12% K₂O (wt%) for SLS scaffold fabrication. The compressive strength of the fabricated scaffolds was studied for up to two months when immersed in Dulbecco's modified eagles medium (DMEM). The compressive strength of the parts decreased from 40 ± 10 MPa in the dry condition and 26 ± 6 MPa after 60 days. Porous biocompatible pure Ti and nitinol (NiTi) alloy was also successfully sintered into 3D scaffold form using a Nd:YAG laser with energy input of $100\text{--}300 \text{ J cm}^{-2}$ [83]. Nd:YAG lasers outperform CO₂ lasers with respect to metallic powders due to better absorbance at shorter wavelengths [84]. Applying the same laser energy during SLS resulted in a much smaller sintered depth of monolayers of NiTi powders compared with pure Ti, which causes lower mechanical strength. On the other hand, it is clear that the SLS parameters significantly affect fabricated tissues. As in previous studies, higher scanning velocity as well as laser power resulted in higher mechanical strength, as shown in table 2. Increasing the value of the scanning velocity prevents delaminating between the layers, resulting in enhancement of mechanical strength. This parameter is significant especially for the fabrication of metallic and alloy tissues by the SLM method.

2.3. Biological properties of SLS parts: *in vitro* and *in vivo* studies

In vitro and *in vivo* tests play an important role in the biological assessment of biomaterials for the fabrication of tissues and scaffolds [87]. A number of architectural characteristics, including porosity, pore size, and permeability, are significant parameters in biological delivery and tissue regeneration. In addition, the materials which are used for tissue engineering must possess a bioactive surface. The ability to control scaffold architecture can provide significant insights into how scaffold architecture and material affect tissue regeneration.

One issue regarding scaffolds made from polymers is the hydrophobic nature of their surface, which results in the negligible availability of bioactive sites [58]. The presence of bioactive binding sites is necessary to induce cell–scaffold adhesion. Chen *et al* [88] have reported a surface modification of PCL scaffolds made by SLS via immersion coating with collagen and gelatin. The collagen-modified scaffold was the best for cartilage tissue engineering in terms of cell proliferation and extracellular matrix production [89]. PCL scaffolds fabricated by SLS can serve as osteoblast or osteogenic scaffolds. They are appropriate scaffolds for the proliferation of adipose-derived stem cells (ASCs) [90]. The addition of bioactive ceramics to hydrophobic but biocompatible polymers is considered beneficial since it reduces the hydrophobicity of the polymer; therefore, it is more favorable for cell attachment and accelerates degradation. The effect of HA addition to a matrix of PCL on MC3T3 osteoblast activity has been examined [71]. The proliferation of adhered cells and the formation of a cell layer on selective laser sintered composites of PCL/HA were observed, and osteoblasts were also encapsulated within the micropores of the struts. The cross sectional images from μ CT confirm a remodeling of up to $\sim 400\ \mu\text{m}$ into the microstructure of the struts. Alamar blue and alkaline phosphate activity (ALP) assays revealed that in general, in the initial period composites with lower HA content (15 wt%) showed better metabolic activity compared with those having higher HA content; however, by day 14 the performance of the two compositions was equal [71].

Das *et al* have fabricated scaffolds from Nylon-6 by SLS [91]. Biocompatibility tests showed that Nylon-6 scaffolds fabricated by SLS support cell viability very well. To investigate the biocompatibility of scaffolds, cells were either in direct contact with the Nylon-6 disks (CoCulture group) or subjected to conditioned media while in contact with the tissue culture polystyrene surface (Conditioned Media group). Two time points were investigated during this study: 3.5 days and 6.5 days in each group. Post-fabrication methods for fabricated scaffolds, e.g., cleaning and treatment, are significant in improving biocompatibility.

In vitro tests of 3D scaffolds have demonstrated that the incorporation of CP nanoparticles significantly improves cell proliferation [19] and alkaline phosphatase activity for CP/PHBV scaffolds, whereas CHA/PLLA nanocomposite scaffolds exhibit a level of cell response comparable to PLLA polymer scaffolds. *In vitro* results have also revealed that the addition of bioactive CS ceramic into a PVA matrix (<20 wt%) enhances the bioactivity of scaffolds, i.e., the number of MG-63 cells attached to the surface of the composites increases in the presence of higher amounts of CS in the scaffolds [79].

Williams *et al* [25] have shown that when taking into account external shape and internal architecture, laser sintered scaffolds can support bone regeneration *in vivo* via gene therapy. Histological evaluation and μ CT data show that the interior pore architecture of laser sintered PCL scaffolds can induce bone generation *in vivo*. Lohfeld *et al* [92] have proposed the use of a biocomposite blend comprising PCL and

TCP prepared by SLS. *In vivo*, a PCL/TCP composite scaffold showed inferior behavior compared with the reference material (β -TCP) with respect to a critical size defect regarding the promotion of bone regeneration, scaffold degradation, and inflammatory reaction. Saito *et al* [93] have examined the effect of biomineral coating on bone regeneration for laser sintered PLLA and PCL scaffolds with the same porous architecture. As a result of bone ingrowth analysis after subcutaneous implantation into mice, coated scaffolds encouraged more penetration of bone interior to the scaffolds than uncoated scaffolds. Cross-sections of the biomineral-coated scaffolds showed good bone contact with the biomineral coatings as well as more bonelike tissue formation, indicating that the biomineral coatings supported direct bone formation rather than fibrous tissue formation.

More studies regarding the biological properties of laser sintered tissues and scaffolds from different materials are summarized in table 3.

3. Inkjet 3DP technology

The binder jetting process is another AM technique which employs inkjet head (IJH) technology for processing materials. In this system, the head prints a liquid binder onto thin layers of powders based on object profiles that have been generated by software [96]. Two kinds of drop-on-demand (DOD) heads can be used in IJH systems: piezoelectric and thermal heads. The main difference between these two heads is their performances. In thermal systems there is a heating element as a thin-film resistor. When an electrical pulse is applied at the head, a high current passes through this resistor and the fluid in contact with it is vaporized, forming a vapor bubble over the resistor. This vapor bubble expands in the fluid reservoir, and the increased pressure causes a droplet to be ejected through the nozzle [97]. In the piezoelectric head system, a volumetric change in the fluid reservoir is induced by the application of a voltage pulse to a piezoelectric material element that is coupled, directly or indirectly, to the fluid. This volumetric change causes pressure/velocity transients to occur within the fluid, and these are directed to produce a drop that issues from the nozzle [98]. Figure 2 shows a layout of the inkjet printing process using both thermal and piezoelectric heads.

Whether to use thermal or piezoelectric inkjet printers depends on the desired properties of the final part. Each inkjet technique has some points which can be categorized as availability, printing speed, accuracy of printed parts, and functional cost. Thermal inkjet printers have some advantages, including availability, higher print speed, and lower cost of parts fabrication compared with piezoelectric inkjet printers [101]. However, the risk of exposing the binder to thermal stress, low droplet directionality, and nonuniform droplet size poses considerable disadvantages with respect to the use of these printers.

On the other hand the advantages of piezoelectric inkjet printers include the capability to generate and control uniform droplet size and ejection directionality as well as to avoid

Table 3. Summary of mechanical and biological properties of laser sintered tissues and scaffolds.

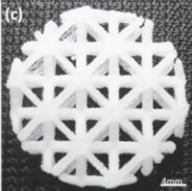
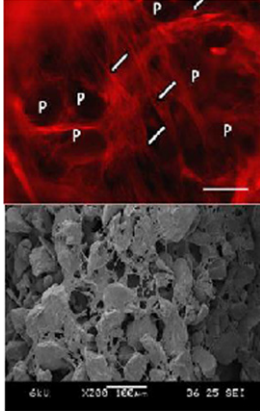
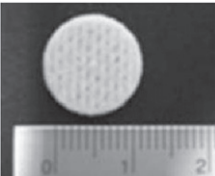
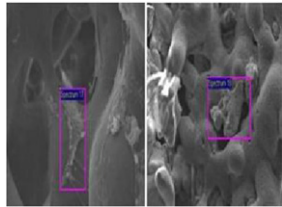
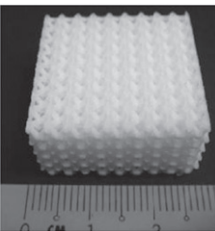
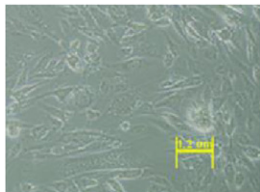
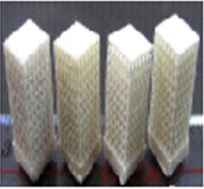
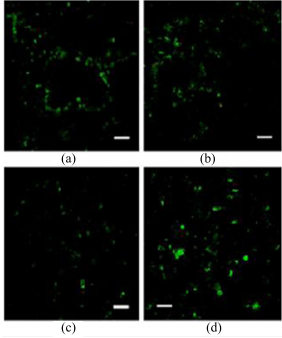

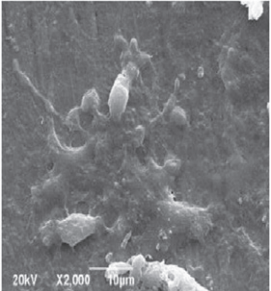
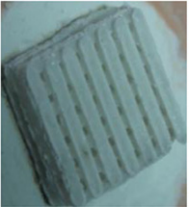
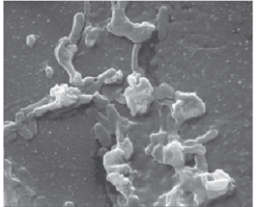
Material	Setup parameters	Physical properties	Mechanical properties	Biological properties	Illustration of final part	Cell images	Reference
PCL ^a	Laser power: 3 W Scanning speed: 3800 mm s ⁻¹	Porosity: 85% Micro- pores: 40–100 micrometers	Tensile strength: 0.43 ± 0.15 MPa Com- pressive strength: :345 kPa	A high density of cells was observed on the scaffold after 6 days.			[46]
PCL	Laser power: 1 W Scanning speed: 500 mm s ⁻¹	Porosity: 83% Micro- pores: 300–400 micrometers	—	The porcine adi- pose-derived stem cells (pASC) pro- liferated well and differentiated into osteoblasts success- fully in the scaffold.			[90]
PCL	Laser power: 3 W Scanning speed: 3810 mm s ⁻¹	Porosity: 40–84%	Tensile strength: 17–5.03 MPa Com- pressive strength: 2.74–5.95 MPa depending on porosity and polyhedral model	A confluent mono- layer of cells with an elongated morphol- ogy could be ob- served on the wells fed with the scaffold extract.			[94]

Table 3. (Continued.)

Material	Setup parameters	Physical properties	Mechanical properties	Biological properties	Illustration of final part	Cell images	Reference
CP /PHBV CHA/PLLA ^b	Laser power for PHBV: 14 W CP/ PHBV: 15 W PLLA: 13 W CHA/LLA: 15 W Scanning Speed: 1257 mm s ⁻¹	Porosity of the PHBV polymer scaffolds: 64.6 ± 2.0% CP/ PHBV scaffolds: 62.6 ± 1.2% PLLA polymer scaffolds: 69.5 ± 1.3% CHA/ PLLA scaffolds: 66.8 ± 2.5%	Compressive strength: PHBV: 0.47 MPa CP/ PHBV: 0.55 MPa PLLA: 0.51 MPa CHA/ PLLA: 0.64 MPa Compressive Young's modulus: PHBV: 4.9 MPa CP/PHBV: 6.6 MPa PLLA: 5.9 MPa CHA/PLLA: 6.2 MPa	All scaffolds were facilitated prolifera- tion of and ALP expression by SaOS- 2 cells. Viability assays of SaOS-2 cells after 3 days of culture on sintered scaffolds			[19]
HA/ β -TCP ^c	Laser power for PHBV: 14 W CP/ PHBV: 15 W PLLA: 13 W CHA/LLA: 15 W Scanning Speed: 1257 mm s ⁻¹	Porosity: 61% Inter- connected macro- porous structure of the scaffold with a rec- tangular pore size range of 0.8–1.2 mm	Fracture toughness: 1.33 MPa m ^{1/2} Com- pressive strength: 18.35 MPa	MG63 cells exhib- ited elongated and flattened morphol- ogy on the TCP/ HAP scaffolds, and the cells were con- nected with cellular micro-extensions			[77]
Forsterite- based scaf- folds with 20% nano- 58S bioactive glass	Laser power: 9.0 W Scan speed: 100.0 mm min ⁻¹	Interconnected porous scaffold with pore size 0.5 to 0.8 mm	Compressive strength: 43.91 MPa	Cells attached and spread well on the forsterite /nano-58S			[95]

^a Polycaprolactone (PCL).^b Calcium phosphate (CP)/poly(hydroxybutyrate-co-hydroxyvalerate) (PHBV) and carbonated hydroxyapatite (CHA)/poly(l-lactic acid) (PLLA) nanocomposite.^c hydroxyapatite (HA) and β -tricalcium phosphate (β -TCP).

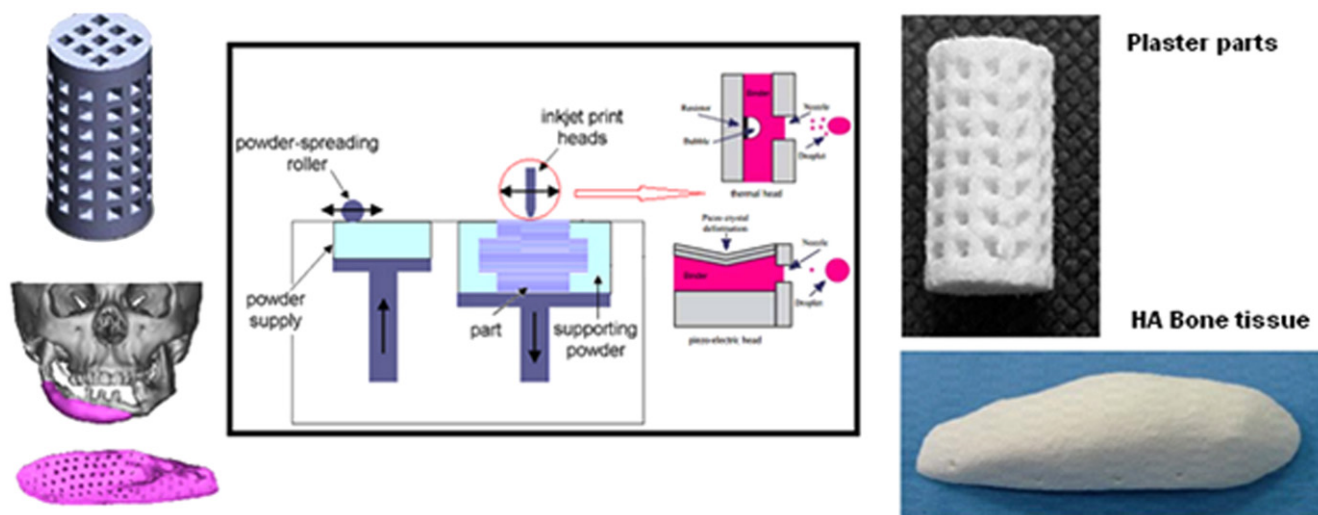


Figure 2. Layout of the inkjet 3DP process. Reproduced with from H Saijo *et al* 2009 *J. Artif. Organs* 12 200–5, with kind permission from Springer Science and Business Media and A Farzadi *et al* 2014 *PloS One* 9 e108252 under a CC BY 4.0 license.

exposure of the binder to heat stressors [102]. The shear stress imposed on the binder at the nozzle tip wall can be avoided by using an open-pool nozzleless ejection system which can also avoid the drawback of nozzle clogging. Adapting piezoelectric printers for less viscous binders in terms of lowering the frequency and power would be challenging since leakage and mist formation during printing may blur the pattern [103, 104].

As the precision of fabricated models strongly depends on the velocity, initial size, and path of the droplets, it is essential to control the parameters, including nozzle diameter, binder properties, and resonance frequency of the head, which have a direct and indirect effect on these terms [102].

3.1. Commonly used materials in inkjet 3DP

In general, a wide range of powders including ceramics and polymers can be processed by inkjet 3DP; however, binder selection is a key factor in successful part fabrication. This section provides a detailed discussion of the existing powders and binders which are used for the fabrication of tissues and scaffolds.

3.1.1. Binders. The materials used as a binder must have suitable properties to prevent spreading from nozzles. To adjust the fluid properties of the organic suspensions to be compatible with the type of printing head, the viscosity and surface tension must be 5–20 Pa.s and 35–40 mJ N⁻¹, respectively. To obtain the aforesaid range, the ratio of $(Re/\sqrt{We} = \sqrt{\sigma\rho r/\eta})$ should be between 1 and 10, where Re is the Reynolds number ($v\mu r/\eta$) and We is the Weber number ($V^2 r\rho/\sigma$). The values ρ , η , and σ are the ink density, viscosity, and surface tension respectively. V and r are droplet velocity and radius respectively [105–107]. When this ratio is too small, viscous forces predominate, which implies high pressure for ejection; inversely, if this ratio is too large, a

continuous column is ejected that can lead to the formation of satellite drops behind the main drop. Figure 3 shows the different cases observed according to the value of (Re/\sqrt{We}) . The binder concentration also plays an important role in inkjet 3DP in achieving the desired dimensional precision [108]. Three different types of binders are commonly used in the inkjet 3DP method: water-based binders such as certain commercial ones (e.g., ZB54, Z Corporation) [100], phosphoric acid-based and citric acid-based binders [109], and polymer solution binders such as PVA and poly(D,L-lactic acid) (PDLLA) [110]. Depending on the type of binder, particles are bonded as the result of adhesive forces or a hydraulic setting reaction; i.e., phosphoric acid can react with tricalcium phosphate powder to produce a matrix of dicalcium phosphate dehydrate.

Although polymeric binders have been widely used to fabricate ceramic parts, the final products suffer low resolution and mechanical strength. Using an acid binder solution has been suggested to improve the resolution and mechanical properties of the printed parts [111]. Lyophilized bovine dermal type I collagen has been added to the phosphoric acid binder to improve the bone healing efficacy of the 3D printed scaffolds. The main concern in using collagen in the binder is the increase in viscosity. To cope with this problem a thermal head with a larger valve diameter must be used, which leads to decreased print resolution [112].

3.1.2. Powders. Flowability of powders is an essential parameter for 3DP processing. Sufficient flowability of powders allows the roller to build up thin layers, leading to high 3DP resolution. Too little flowability decreases fabrication resolution due to insufficient recoating. On the other hand, very high flowability does not provide sufficient powder bed stability for 3DP.

Wettability of particles is another factor in 3DP processing. The volume of binder distributed into the powder

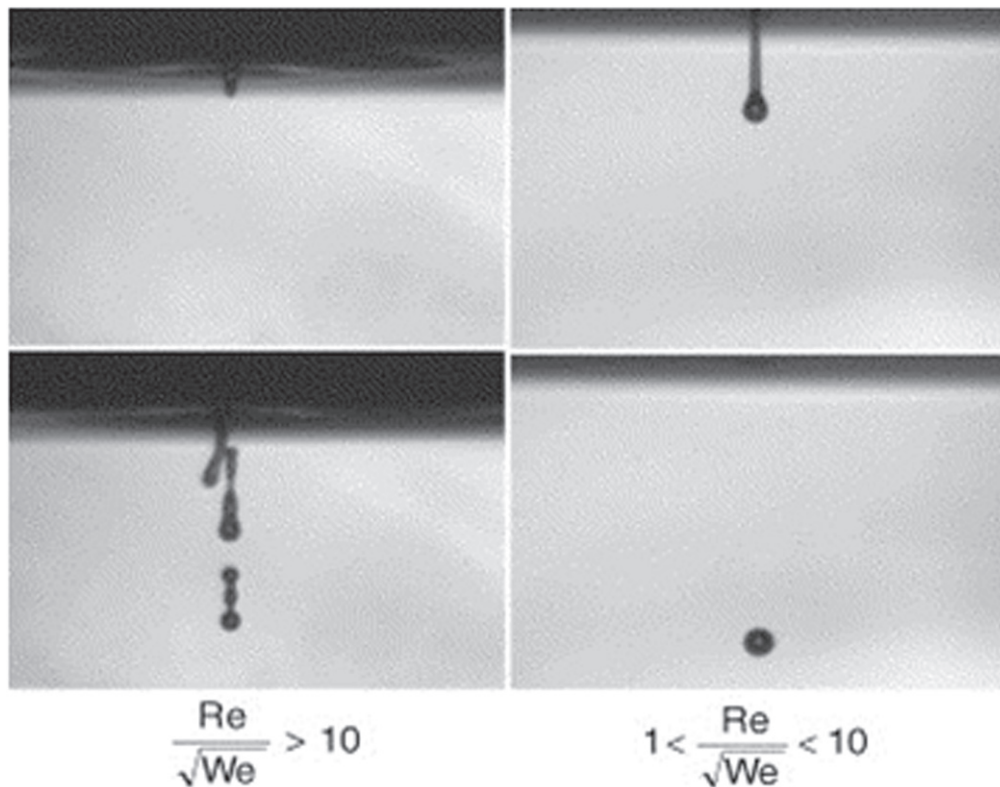


Figure 3. Ejection images of suspensions showing the effect of the ratio of (Re/\sqrt{We}) . Reprinted from R Noguera *et al* 2005 *J. Eur. Ceram. Soc.* 25 2055–9, Copyright 2005, with permission from Elsevier.

bed and also the amount of binder absorbed by the powders determines the resolution (voxel size) and mechanical properties of the parts. It has been confirmed that too-low wetting of fine powder particles results in powder bed rearrangement that is possibly detrimental to further 3DP, and too-high wetting and slow powder reaction will reduce the smallest feature size [113–115]. The particle size of powders also has an effect on the mechanical strength of the printed parts. Changing the powder particle size alters the pore size distribution within the powder bed, which influences the drop penetration behavior of a water-based binder [116].

For powder materials, a broad range of polymers, ceramics, and composites can be applied in the field of tissue engineering. As has been previously described the binding mechanism of bioceramic powders used in binder jetting systems is based on the hydraulic setting reaction [117–119]. When dry hydraulic cement is mixed with water, chemical reactions happen in the composite which cause the formation of a firm ceramic-based composite. Because of the nature of the compounds formed in these reactions, they are insoluble in water. This means that the hardened cement will retain its strength and hardness even if immersed in water.

CP has been widely applied in inkjet printing [73, 120]. CP powders can be bound by aqueous (often acidic) binder solutions through a dissolution–precipitation reaction [121]. Solution of a soluble polymeric binder [122, 123] can be used for wet ceramic particles and can glue them together through drying. After the printing process, functioned parts are

depowdered and the organic binder removed during sintering [123–125]. Table 4 summarizes the most commonly used powder materials and binders for the production of tissues and scaffolds.

3.2. Mechanical properties of inkjet 3DP parts

Improving the mechanical properties of porous parts is a challenge in inkjet 3DP. In some cases, to reach a suitable strength, the scaffolds are sintered after printing. This post-processing exposes the final part to failure due to the burnout of binder which is present or because of high binder concentration. Therefore, the binder concentration must be minimized while still providing sufficient mechanical stability to the printed structure. Moreover, sintering causes a dimensional change in the final part [134]. Tarafder *et al* [135] have reported a significant increase in the mechanical strength of macroporous TCP scaffolds via microwave sintering compared with conventional sintering. Saijo *et al* [99] have fabricated parts with sufficient mechanical strength without using the sintering process. They propose that a reasonable mechanical strength for ceramic scaffolds can be achieved by optimizing the particle size of the powder and the pH and viscosity of the binder.

As mentioned in section 3.1.1, different experiments have been carried out to study the influence of binders on the properties of fabricated parts. In a study of the fabrication of 3D porous strontium-containing mesoporous bioactive glass

Table 4. Powders and binders used for tissue engineering.

Material	Particle size (μm)	Binder	Reference
Plaster-based powder	~ 27 (d_{50})	Water-based solution with 2-pyrrolidone	[100]
High-density polyethylene (HDPE)	80–100	Maltodextrin + poly(vinyl alcohol) + lecithin	[126]
Polyethylene + maltodextrin	100–150	Distilled water	[127]
Cornstarch + Dextran + Gelatin	–	Distilled water + blue dye	[128]
TCP + TTCP ^a	10–20	10–20% phosphoric acid	[129]
β -TCP	16 (d_{50})	25% oxalic + tartaric acid	[130]
α -TCP	30	5% sodium chondroitin sulfate	
		12% disodium succinate	[131]
		83% distilled water	
Calcium silicate	0.3–5	12% polyvinyl alcohol solution	[110]
CP	30–50	8.75% Phosphoric acid	[132]
	50–150		
HA + CaSO ₄	<20 (d_{90}) ≥ 20 (d_{10})	Commercial water-based (ZB7)	[133]

^a Tetracalcium phosphate (TTCP)

scaffolds, the 3D printed scaffolds exhibited greater compressive strength (8–9 MPa) than the compressive strength of human trabecular bone (2–12 MPa) [136]. In addition, the mechanical strength of a scaffold could be maintained at approximately 7 MPa after soaking in simulated body fluid (SBF). These results are attributed to the use of aqueous PVA binder, which bonds the ceramic particles together and consequently decreases the brittleness of the scaffolds. Wu *et al* [110] have prepared a β -CS scaffold using 12% PVA solution as a binder. The compressive strength and Young's modulus of printed CS scaffolds with a pore size of 1×1 mm and porosity of 65% were 3.6 ± 0.1 MPa and 40 ± 8 MPa. A study of the deformation of scaffolds during the compressive test revealed that the printed CS scaffolds partially maintained a scaffold configuration in the center position and only the border area collapsed. This may be interpreted as the effect of the proper distribution of polymeric binder on the flexibility of the printed scaffolds.

By comparing the compressive strength of CS scaffolds with those using polyurethane (PU) foam and PDLA solutions to bind the particles, the influential role of binders in inkjet 3DP can be seen. The strengths of scaffolds prepared using PU and PDLA solutions as binders were 0.3 and 1.45 MPa, respectively, i.e., significantly lower than when using a PVA solution [137].

In the case of acidic binders, Vorndran *et al* [111] have fabricated parts from β -TCP as the powder and phosphoric acid as the binder. They improved the compressive strength by adjusting the volume ratio of binder to powder. Compressive strengths of 3.4 and 7.4 MPa were obtained for a binder-to-powder-volume ratio of 2 and 4, respectively. Another study showed that an 8.75 wt% phosphoric acid solution binder can improve mechanical strength while retaining cell viability at $68\% \pm 6\%$. As a surfactant, 0.25 wt% Twin 80 was added to the binder solution to improve printability [132].

As mentioned earlier, the size of the powder particles has a direct influence on the mechanical strength of the parts. In HA/CaSO₄ (calcium sulfate) composites it was confirmed that

using very fine HA powders ($\leq 20 \mu\text{m}$) leads to a loosely packed powder bed and thus a high level of heterogeneity, which results in slow drop penetration, large drop penetration depth, low wetting ratio, and poor green mass and green strength for the final 3DP components. On the other hand, using coarser HA powders (30–100 μm) can show higher mechanical strength values [133]. Printing the parts along different axes also has an effect on mechanical strength. Composites of HA/PVA as bone tissue have shown different mechanical behaviors along different printing axes [138]. The mechanical strength for X-axis scaffolds has been reported as 0.76 ± 0.02 MPa, whereas this value is 0.88 ± 0.02 MPa along the Y-axis. Despite exhibiting a higher compressive strength, scaffolds printed along the Y-axis have been shown to contain traces of PVA degradation products after heat treatment. Using metal oxide components as a reinforcement agent is also recommended to improve the mechanical properties of bioactive ceramics, especially for hard tissues and implant applications [139, 140]. Moreover, the addition of SiO₂/ZnO to TCP can increase the mechanical properties of implants. For investigation of this effect, Fielding *et al* [120] fabricated a cylindrical scaffold by binder jetting with the addition of SiO₂/ZnO. Cylindrical scaffold CAD files were created with interconnected square channels of 1000 μm , 750 μm , and 500 μm sides and 7 mm diameter and 10.5 mm height. The doped fabricated scaffolds, which had less total open pore volume than the pure scaffolds, showed the greatest compressive strength, with the 1000 μm , 750 μm , and 500 μm green channel sizes at 10.21 ± 0.11 MPa, 8.2 ± 0.4 MPa, and 4.34 ± 0.3 MPa, respectively. The pure samples with the green channel sizes 1000 μm , 750 μm , and 500 μm had average compressive strengths of 5.48 ± 0.04 MPa, 2.7 ± 0.2 MPa, and 1.8 ± 0.2 MPa, respectively.

3.3. Biological properties of inkjet 3DP parts: *in vitro* and *in vivo* studies

Apart from having good mechanical properties, tissues and scaffolds fabricated by inkjet 3DP must be able to react with

cells after implantation. Improving the biological properties (biocompatibility, biodegradability, and cell proliferation) of printed tissues depends on the properties of powders and binders, on pore volume, and also on post-processing of printed tissues.

As previously discussed, in some cases poor mechanical strength of printed tissues can be improved by the sintering process. However, sintering may also compromise biodegradability due to increases in the crystallinity of printed parts, leading to poor resorption by osteoclasts [99]. The binder properties also play a crucial role in the biological properties. The effect of binder solution acidity on the biological properties of printed calcium phosphate scaffolds has been demonstrated by Inzana *et al* [132]. Although higher acidity of binders results in greater mechanical strength of scaffolds, it also increases toxicity. Phosphoric acid of 12.5 wt% almost leads to cell death due to the pH of media falling below 5 [132].

A report by Becker *et al* [141] has presented the prototyping of three scaffolds of HA, TCP, and TCP and bovine HA composites by binder jetting technology. Aqueous solutions of dextrin (20 wt%) and saccharose (2.5 wt%) were used as the binder. After *in vivo* tests and cell seeding, it was concluded that 3D-printed hydroxyapatite and 3D-printed TCP as well as bovine HA blocks are biocompatible for cells derived from a human periosteum.

Studies have shown that zinc oxide has a stimulatory influence on fabricated tissue formation *in vitro* and *in vivo* and also increases the ALP of TCP/zinc oxide composite, which is an enzymatic marker for osteoblastic differentiation [142, 143].

Since bone can grow into pores with a diameter of approximately 300 μm , providing pores of this size or larger is essential for bone grafting. Depending on whether post-processing is used, pores with the desirable geometry can be created by considering the pore size and geometry in the primary design of the structure or can be derived from porogens burned out during sintering. Pore geometry is known to be an important factor in determining bone healing response [144]. The addition of dopants in bioactive ceramics such as TCP can also affect osteogenic differentiation via modification of pore size. Although in many cases cation substitutions such as Na^+ , Mg^{2+} , and Sr^{2+} have led to excellent improvement in the biological properties of HA, only a few studies have investigated the effect of cation doping on the 3D interconnected porosity of 3D printed tissues and scaffolds. Both micro and interconnected macropores facilitate the infiltration of osteoprogenitor cells, which emphasizes the presence of multiscale porosity in tissue engineering scaffolds. In a research conducted by Tarafder *et al* [145], the presence of Mg^{2+} and Sr^{2+} in a TCP structure and their influence on 3D printed bone tissues led to pore sizes of $245 \pm 8 \mu\text{m}$ and $311 \pm 6 \mu\text{m}$ for doped and pure TCP scaffolds, respectively, which were close to the designed pore size of 350 μm [145]. As shown in figure 4, improvement of bone formation inside macropores (when tested in rat femoral defects) was observed in microwave sintered Mg/Sr-doped TCP tissues. Interconnected pores made by inkjet 3DP result

in good cell–tissue reaction, which leads to the development of new bone formation and bone remodeling inside the interconnected macropores and intrinsic micropores of 3D printed scaffolds.

Another *in vivo* study has also revealed the effect of pores on bone formation after implantation, i.e., cylindrical holes 2 mm in diameter running across 3D printed tailor-made bone implants (TIs) showed that bone formation on a larger scale was facilitated [131]. Based on computed tomography (CT) analysis of the skulls of beagle dogs, the volume of the cylindrical holes decreased after the operation, and histological analysis revealed that newly formed bone tissue had invaded the cylindrical holes. Not only can TIs fabricated by an inkjet 3D printer facilitate bone healing due to the excellent natural properties of TCP, but a properly designed hole in the implant structure can also improve bone healing [131].

4. Key issues and challenges to clinical applications

AM offers unique advantages with respect to fabrication tissues and scaffolds with a complex external anatomy shape and internal porous structure. Coupling complicated porous 3D design with AM techniques can create a range of bone tissues and scaffolds from various materials. Among the AM techniques, inkjet 3DP and SLS are two powder-based tools which are widely used for biomedical engineering applications.

In the case of SLS, the initial setting, e.g., laser power and scanning speed, is crucial. Without any modification, commercial SLS machines can be used only for small amounts of powdered materials for fabricating specific biomedical applications. Different research groups have begun to optimize the SLS parameters for fabricating special objects with a desired 3D porous architecture in minimum fabrication time and at minimal cost. For tissue engineering, control over mechanical behavior while retaining the designed porous structure is very important. This issue can restrict the use of pure biocompatible polymers. Another disadvantage of the SLS technique for scaffold fabrication is that hydrogels cannot be processed, and it is also impossible to encapsulate cells in scaffolds [84]. The lack of vascularization within scaffolds is still a major concern for scaffolds targeting specific tissue regeneration. Non-fine feature resolution of the SLS technique is a particular drawback which can affect fabricated tissues in terms of cell seeding and growth-factor delivery.

In the case of using inkjet 3DP machines for tissue engineering, although this method can be employed for fabricating tissues with defined shapes and porous architecture from almost all ceramics and polymer materials, the selecting of a suitable binder is still a challenge which needs extensive optimization. Among the binders, acidic ones can provide good mechanical properties for fabricated tissues; however, binder residue in printed structures is difficult to remove and may make tissues toxic. In most cases, post-processing such as sintering is required for printed parts to achieve the desired mechanical behavior. During the sintering process, parts shrink, and unfortunately the shrinkage

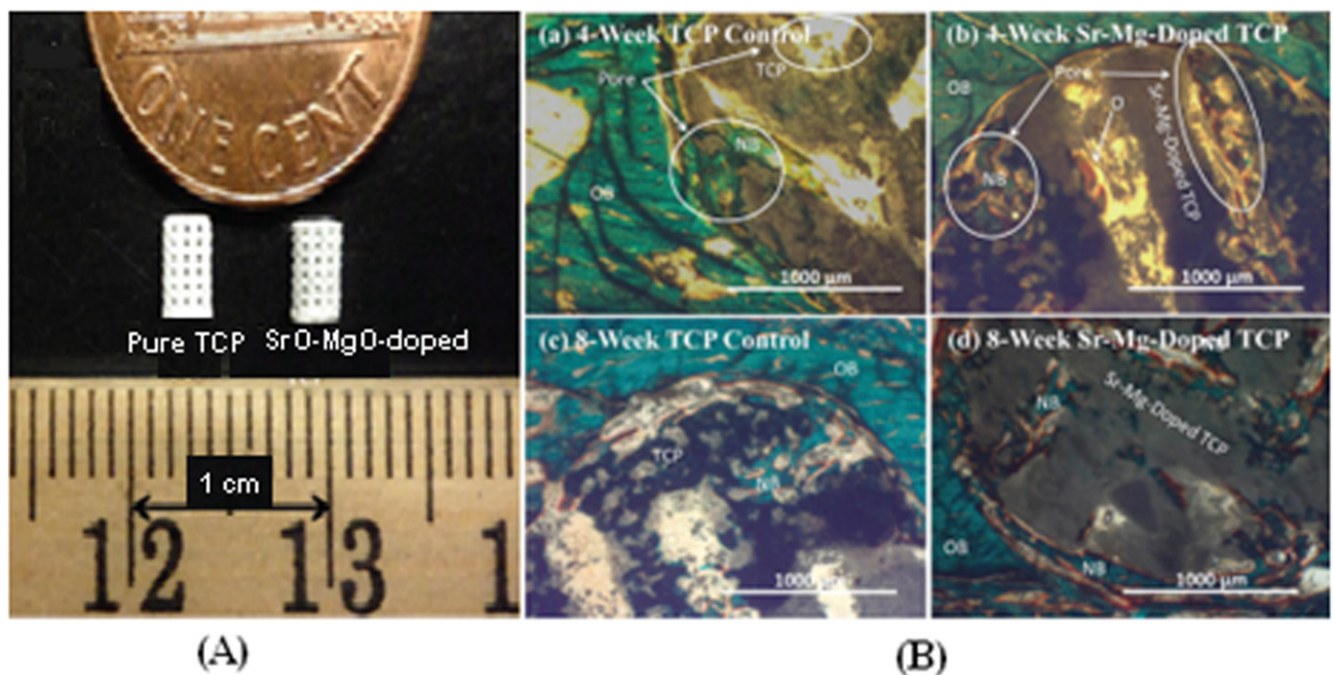


Figure 4. (A) 3D printed tissues; (B) microscopy image of (a) and (c) 3DP pure TCP implants and (b) and (d) Sr/Mg-doped TCP implants, showing the development of new bone formation and bone remodeling inside the interconnected macro and intrinsic micro pores of 3DP scaffolds after four and eight weeks in a rat distal femur model. Modified Masson–Goldner trichrome staining of transverse section. OB: old bone, NB: new bone, O: osteoid, and BM: bone marrow. Color description: dark gray/black = scaffold; orange/red = osteoid; green/bluish = new mineralized bone (NMB)/old bone. Reproduced from S Tarafder *et al* 2013 *Biomater. Sci.* **1** 1250–9, with permission of The Royal Society of Chemistry.

is not necessarily uniform. The first effect of non-uniform shrinkage on sintered parts is cracking, which make the parts useless. Since the outside part of bone is denser than the inner part, mimicking such structures is very difficult using 3DP, which is the second challenge related to non-uniform shrinkage during sintering [146]. Another post-processing challenge is the removal of loose powders from interconnected pores inside the part. This problem is highlighted for structures with small pores ($<600\ \mu\text{m}$). Trapped powders inside the pores may well sinter with the porous part, making it less interconnected than the designed part. Such problems with loose powders can reduce the dimension of the pores after sintering.

Apart from the issues related to SLS and inkjet 3DP settings as well as selecting suitable biomaterials, clinical usage of AM processed parts is still a big challenge. In fact, there are many obstacles along this long and difficult road.

The gap between the concept and the clinical use of tissue engineering comprises three main factors: the need for understanding native-tissue characterization, the need to incorporate this characterization into tissue design, and finally, the necessity of fabricating tissues based on these design specifications. Despite all the advances in biomaterials science, there are still major gaps in this field relative to the surface chemistry, growth factor release, and mass-transport characteristics that best accelerate a specific tissue formation. Therefore, there are no strategies specifying which material is

appropriate for tissues, which linear or nonlinear elastic properties a scaffold should exhibit, which surface chemistry a scaffold should have, or which permeability or diffusion properties a scaffold should demonstrate. In addition to these gaps and challenges, the clinical use of artificial tissues and scaffolds needs volunteer patients for bone tissue replacement surgeries. Because this field is still new and not much clinical surgery has been done, this high-risk surgery might pose challenges after implantation.

Few SLS and ink jet printing products have been used in clinical applications. Most reports have been limited to using models as guide templates for surgery and for *in vitro* and *in vivo* experiments, whereas implantations of scaffolds in the human body are still rare. The union between produced parts and host bones is affected by dimensional compatibility, biodegradability, pore size, and pore interconnectivity. Saijo *et al* [99] have reported a maxillofacial reconstruction by using a custom-made artificial bone made by an inkjet printer. The bone was fabricated with a macropore structure and no sintering process, using α -TCP powder with $10\ \mu\text{m}$ particle diameter and a mixture of 5% sodium chondroitin sulfate, 12% disodium succinate, and 83% distilled water as a curing solution. The scaffolds showed rapid union in 10 patients at 12 months after implantation, which can be attributed to the implant macropore structure resulting in rapid cell growth [147]. Recently Mangano *et al* [148] reported a clinical use of SLS titanium (master alloy powder (Ti6Al4V)) blade implants as

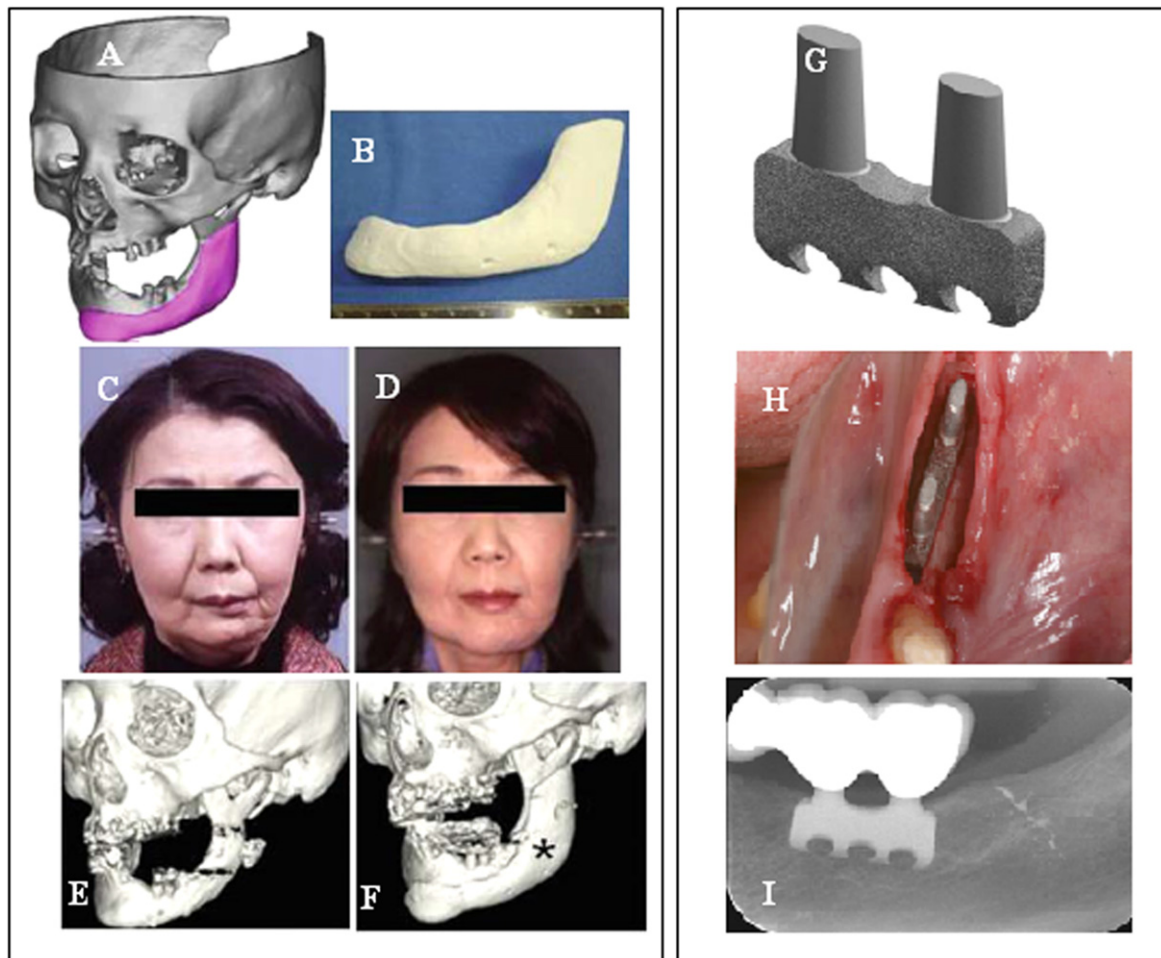


Figure 5. Clinical application of custom-made artificial bone from α -TCP using inkjet 3D printing (left) (reproduced from H Saijo *et al* 2009 *J. Artif. Organs* **12** 200–5, with kind permission from Springer Science and Business Media) and custom-made SLS titanium blade implants (right) (reproduced from F Mangano *et al* 2013 *Lasers Med. Sci.* **28** 1241–7, with kind permission from Springer Science and Business Media). Left: (A) Extraction of the CAD data of the created artificial bone (red) based on a CT image. (B) Macroscopic image of the inkjet-printed custom-made artificial bone (IPCAB). (C) Facial appearance 1 year after surgery. (D) 3D CT image of the left lower jaw before surgery. (E) 3D CT image of the left lower jaw 12 months after surgery. Right: (G) CAD file of the custom-made SLS titanium blade implant. (H) The custom-made SLS blade implant placed in position. (I) The radiographic control two years after implant placement.

a non-conventional solution for the prosthetic rehabilitation of extremely atrophied posterior mandibles. Two years after loading, all implants were in good condition and demonstrated perfect aesthetic integration. Compared with conventional approaches such as bone reconstructive surgery, the use of cost-effective SLS implants as a therapeutic treatment can represent an alternative for elderly patients because of lower morbidity. Figure 5 illustrates such custom-made artificial bones fabricated through the use of inkjet 3DP and SLS for clinical applications.

Demand for AM technologies such as SLS and 3DP will increase in the future due to their capability to make custom medical devices that can be tailored for patient-specific and defect-specific clinical needs. Integrating all key points mentioned as well as finding solutions to cope with the challenges and issues are important in guiding the progress of these techniques toward achieving the objective of clinical use.

Acknowledgments

This study was funded by the Ministry of Higher Education of Malaysia (MOHE), Grant Number UM.C/HIR/MOHE/ENG/10 D00010-16001, entitled ‘Biomechanical System for Hard Tissues of Normal and Disable Subjects’, and research grant numbers IPP PG012-2012B and UMRG RP021-2012A, supported by the University of Malaya. The authors are also grateful for further support from the ‘Bright Spark’ Unit.

References

- [1] Hutmacher D W, Sittiger M and Risbud M V 2004 Scaffold-based tissue engineering: rationale for computer-aided design and solid free-form fabrication systems *Trends Biotechnol.* **22** 354–62

- [2] Pham D T and Gault R S 1998 A comparison of rapid prototyping technologies *Int. J. Mach. Tools Manuf.* **38** 1257–87
- [3] Wendel B, Rietzel D, Kühnlein F, Feulner R, Hülder G and Schmachtenberg E 2008 Additive processing of polymers *Macromol. Mater. Eng.* **293** 799–809
- [4] Melchels F P W, Feijen J and Grijpma D W 2010 A review on stereolithography and its applications in biomedical engineering *Biomaterials* **31** 6121–30
- [5] Onuh S O and Yusuf Y Y 1999 Rapid prototyping technology: applications and benefits for rapid product development *J. Intell. Manuf.* **10** 301–11
- [6] Gibson I, Rosen D W and Stucker B 2010 *Additive Manufacturing Technology* (New York: Springer)
- [7] Warnke P H, Seitz H, Warnke F, Becker S T, Sivananthan S, Sherry E, Liu Q, Wiltfang J and Douglas T 2010 Ceramic scaffolds produced by computer-assisted 3D printing and sintering: characterization and biocompatibility investigations *J. Biomed. Mater. Res. B: Appl. Biomater.* **93B** 212–7
- [8] Rahmati S, Abbaszadeh F and Farahmand F 2012 An improved methodology for design of custom-made hip prostheses to be fabricated using additive manufacturing technologies *Rapid Prototyping J.* **18** 389–400
- [9] Bohner M, van Lenthe G H, Grunenfelder S, Hirsiger W, Evison R and Muller R 2005 Synthesis and characterization of porous beta-tricalcium phosphate blocks *Biomaterials* **26** 6099–105
- [10] Ko S H, Pan H, Grigoropoulos C P, Luscombe C K, Fréchet J M J and Poulikakos D 2007 All-inkjet-printed flexible electronics fabrication on a polymer substrate by low-temperature high-resolution selective laser sintering of metal nanoparticles *Nanotechnology* **18** 345202
- [11] Kruth J P, Vandenbroucke B, Van Vaerenbergh J and Naer I 2005 Rapid manufacturing of dental prostheses by means of selective laser sintering/melting *Proc. AFPR, S4* (Netherlands)
- [12] Silva D N, Gerhardt de Oliveira M, Meurer E, Meurer M I, Lopes da Silva J V and Santa-Bárbara A 2008 Dimensional error in selective laser sintering and 3D-printing of models for craniomaxillary anatomy reconstruction *J. Cranio-Maxillofacial Surg.* **36** 443–9
- [13] Eshraghi S and Das S 2010 Mechanical and microstructural properties of polycaprolactone scaffolds with one-dimensional, two-dimensional, and three-dimensional orthogonally oriented porous architectures produced by selective laser sintering *Acta Biomater.* **6** 2467–76
- [14] Sallica-Leva E, Jardini A L and Fogagnolo J B 2013 Microstructure and mechanical behavior of porous Ti–6Al–4 V parts obtained by selective laser melting *J. Mech. Behav. Biomed. Mater.* **26** 98–108
- [15] Vaezi M, Seitz H and Yang S 2013 A review on 3D micro-additive manufacturing technologies *Int. J. Adv. Manuf. Technol.* **67** 1721–54
- [16] Shuai C, Zhuang J, Peng S and Wen X 2014 Inhibition of phase transformation from β -to α -tricalcium phosphate with addition of poly (L-lactic acid) in selective laser sintering *Rapid Prototyping J.* **20** 369–76
- [17] Kolan K C, Leu M C, Hilmas G E and Velez M 2012 Effect of material, process parameters, and simulated body fluids on mechanical properties of 13–93 bioactive glass porous constructs made by selective laser sintering *J. Mech. Behav. Biomed. Mater.* **13** 14–24
- [18] Salmoria G V, Klauss P, Paggi R A, Kanis L A and Lago A 2009 Structure and mechanical properties of cellulose based scaffolds fabricated by selective laser sintering *Polym. Test.* **28** 648–52
- [19] Duan B, Wang M, Zhou W Y, Cheung W L, Li Z Y and Lu W W 2010 Three-dimensional nanocomposite scaffolds fabricated via selective laser sintering for bone tissue engineering *Acta Biomater.* **6** 4495–505
- [20] Savalani M M, Hao L, Dickens P M, Zhang Y, Tanner K E and Harris R A 2012 The effects and interactions of fabrication parameters on the properties of selective laser sintered hydroxyapatite polyamide composite biomaterials *Rapid Prototyping J.* **18** 16–27
- [21] Amorim F L, Lohrengel A, Neubert V, Higa C F and Czelusniak T 2014 Selective laser sintering of Mo–CuNi composite to be used as EDM electrode *Rapid Prototyping J.* **20** 59–68
- [22] Gu D and Shen Y 2008 Influence of Cu-liquid content on densification and microstructure of direct laser sintered submicron W–Cu/micron Cu powder mixture *Mater. Sci. Eng.: A* **489** 169–77
- [23] Feng P, Niu M, Gao C, Peng S and Shuai C 2014 A novel two-step sintering for nano-hydroxyapatite scaffolds for bone tissue engineering *Sci. Rep.* **4** 5599
- [24] Tan K H, Chua C K, Leong K F, Cheah C M, Cheang P, Abu Bakar M S and Cha S W 2003 Scaffold development using selective laser sintering of polyetheretherketone–hydroxyapatite biocomposite blends *Biomaterials* **24** 3115–23
- [25] Williams J M, Adewunmi A, Schek R M, Flanagan C L, Krebsbach P H, Feinberg S E, Hollister S J and Das S 2005 Bone tissue engineering using polycaprolactone scaffolds fabricated via selective laser sintering *Biomaterials* **26** 4817–27
- [26] Goodridge R D, Tuck C J and Hague R J M 2012 Laser sintering of polyamides and other polymers *Prog. Mater. Sci.* **57** 229–67
- [27] Sachdeva A, Singh S and Sharma V 2013 Investigating surface roughness of parts produced by SLS process *Int. J. Adv. Manuf. Technol.* **64** 1505–16
- [28] Gu D and Shen Y 2009 Effects of processing parameters on consolidation and microstructure of W–Cu components by DMLS *J. Alloys Compd.* **473** 107–15
- [29] Walker D C, Caley W F and Brochu M 2014 Selective laser sintering of composite copper–tin powders *J. Mater. Res.* **29** 1997–2005
- [30] Wang J, Yang M and Zhang Y 2014 A nonequilibrium thermal model for direct metal laser sintering *Numer. Heat. Tr. A—Appl.* **67** 249–67
- [31] Asgharzadeh H and Simchi A 2005 Effect of sintering atmosphere and carbon content on the densification and microstructure of laser-sintered M2 high-speed steel powder *Mater. Sci. Eng.: A* **403** 290–8
- [32] Gu D D and Shen Y F 2006 Influence of phosphorus element on direct laser sintering of multicomponent Cu-based metal powder *Metall. Mater. Trans. B* **37** 967–77
- [33] Kruth J-P, Kumar S and Van Vaerenbergh J 2005 Study of laser-sinterability of ferro-based powders *Rapid Prototyping J.* **11** 287–92
- [34] Das S, Beama J J, Wohlert M and Bourell D L 1998 Direct laser freeform fabrication of high performance metal components *Rapid Prototyping J.* **4** 112–7
- [35] Ajoku U, Hopkinson N and Caine M 2006 Experimental measurement and finite element modelling of the compressive properties of laser sintered Nylon-12 *Mater. Sci. Eng.: A* **428** 211–6
- [36] Bicerano J and Seitz J T 1996 Molecular origins of toughness in polymers *Polymer Toughening* (New York: Dekker) pp 1–59
- [37] Wisanrakkit G and Gillham J 1990 The glass transition temperature (T_g) as an index of chemical conversion for a high- T_g amine/epoxy system: chemical and diffusion-

- controlled reaction kinetics *J. Appl. Polym. Sci.* **41** 2885–929
- [38] Kruth J P, Levy G, Klocke F and Childs T H C 2007 Consolidation phenomena in laser and powder-bed based layered manufacturing *CIRP Ann—Manuf. Technol.* **56** 730–59
- [39] Schmidt M, Pohle D and Rechtenwald T 2007 Selective laser sintering of PEEK *CIRP Ann—Manuf. Technol.* **56** 205–8
- [40] Ho H C H, Cheung W L and Gibson L 2002 Effects of graphite powder on the laser sintering behaviour of polycarbonate *Rapid Prototyping J.* **8** 233–42
- [41] Beaman J J, Barlow J W, Bourell D L, Crawford R H, Marcus H L and McAlea K P 1997 *Solid Freeform Fabrication: A New Direction in Manufacturing* (Dordrecht: Kluwer Academic)
- [42] Gharekhani S, Sadeghinezhad E, Kazi S N, Yarmand H, Badarudin A, Safaei M R and Zubir M N M 2015 Basic effects of pulp refining on fiber properties—a review *Carbohydrate Polym.* **115** 785–803
- [43] Gunatillake P A and Adhikari R 2003 Biodegradable synthetic polymers for tissue engineering *Eur. Cells Mater.* **5** 1–16
- [44] Sabir M I, Xu X and Li L 2009 A review on biodegradable polymeric materials for bone tissue engineering applications *J. Mater. Sci.* **44** 5713–24
- [45] Mkhabela V J and Ray S S 2014 Poly (ϵ -caprolactone) nanocomposite scaffolds for tissue engineering: a brief overview *J. Nanosci. Nanotechnol.* **14** 535–45
- [46] Yeong W, Sudarmadji N, Yu H, Chua C, Leong K, Venkatraman S, Boey Y and Tan L 2010 Porous polycaprolactone scaffold for cardiac tissue engineering fabricated by selective laser sintering *Acta Biomater.* **6** 2028–34
- [47] Bertrand P, Bayle F, Combe C, Goeuriot P and Smurov I 2007 Ceramic components manufacturing by selective laser sintering *Appl. Surf. Sci.* **254** 989–92
- [48] Hagedorn Y C, Balachandran N, Meiners W, Wissenbach K and Poprawe R 2011 SLM of net-shaped high strength ceramics: new opportunities for producing dental restorations *Proc. Solid Freeform Fabrication Symp. (Austin, TX)* pp 8–10
- [49] Tang H-H, Chiu M-L and Yen H-C 2011 Slurry-based selective laser sintering of polymer-coated ceramic powders to fabricate high strength alumina parts *J. Eur. Ceram. Soc.* **31** 1383–8
- [50] Shahzad K, Deckers J, Kruth J-P and Vleugels J 2013 Additive manufacturing of alumina parts by indirect selective laser sintering and post processing *J. Mater. Process. Technol.* **213** 1484–94
- [51] Liu F-H 2014 Synthesis of biomedical composite scaffolds by laser sintering: Mechanical properties and *in vitro* bioactivity evaluation *Appl. Surf. Sci.* **297** 1–8
- [52] Liu X, Morra M, Carpi A and Li B 2008 Bioactive calcium silicate ceramics and coatings *Biomed. Pharmacother.* **62** 526–9
- [53] Shuai C, Feng P, Yang B, Cao Y, Min A and Peng S 2014 Effect of nano-zirconia on the mechanical and biological properties of calcium silicate scaffolds *Int. J. Appl. Ceram. Technol.* at press (doi:10.1111/ijac.12337)
- [54] Hazar A B Y 2007 Preparation and *in vitro* bioactivity of CaSiO₃ powders *Ceram. Int.* **33** 687–92
- [55] Shirazi F S, Moghaddam E, Mehrali M, Oshkour A A, Metselaar H S C, Kadri N A, Zandi K and Abu N A 2014 *In vitro* characterization and mechanical properties of β -calcium silicate/POC composite as a bone fixation device *J. Biomed. Mater. Res. A* **102** 3973–85
- [56] Shuai C, Mao Z, Han Z, Peng S and Li Z 2014 Fabrication and characterization of calcium silicate scaffolds for tissue engineering *J. Mech. Med. Biol.* **14** 1450049
- [57] Tan K, Chua C, Leong K, Cheah C, Cheang P, Bakar M A and Cha S 2003 Scaffold development using selective laser sintering of polyetheretherketone–hydroxyapatite biocomposite blends *Biomaterials* **24** 3115–23
- [58] Wiria F, Leong K, Chua C and Liu Y 2007 Poly- ϵ -caprolactone/hydroxyapatite for tissue engineering scaffold fabrication via selective laser sintering *Acta Biomater.* **3** 1–12
- [59] Shahzad K, Deckers J, Zhang Z, Kruth J-P and Vleugels J 2014 Additive manufacturing of zirconia parts by indirect selective laser sintering *J. Eur. Ceram. Soc.* **34** 81–9
- [60] Drummer D, Rietzel D and Kühnlein F 2010 Development of a characterization approach for the sintering behavior of new thermoplastics for selective laser sintering *Phys. Proc.* **5** 533–42
- [61] Bose S, Roy M and Bandyopadhyay A 2012 Recent advances in bone tissue engineering scaffolds *Trends Biotechnol.* **30** 546–54
- [62] Gao C, Liu T, Shuai C and Peng S 2014 Enhancement mechanisms of graphene in nano-58 S bioactive glass scaffold: mechanical and biological performance *Sci. Rep.* **4** 4712
- [63] Xynos I D, Hukkanen M V J, Batten J J, Buttery L D, Hench L L and Polak J M 2000 Bioglass (R) 45S5 stimulates osteoblast turnover and enhances bone formation *in vitro*: implications and applications for bone tissue engineering *Calcif. Tissue Int.* **67** 321–9
- [64] Boccaccini A R, Erol M, Stark W J, Mohn D, Hong Z K and Mano J F 2010 Polymer/bioactive glass nanocomposites for biomedical applications: a review *Compos. Sci. Technol.* **70** 1764–76
- [65] Wheeler D L, Montfort M J and McLoughlin S W 2001 Differential healing response of bone adjacent to porous implants coated with hydroxyapatite and 45S5 bioactive glass *J. Biomed. Mater. Res.* **55** 603–12
- [66] Huang Y, Han S, Pang X, Ding Q and Yan Y 2013 Electrodeposition of porous hydroxyapatite/calcium silicate composite coating on titanium for biomedical applications *Appl. Surf. Sci.* **271** 299–302
- [67] Hedberg Y S, Qian B, Shen Z, Virtanen S and Odnevall Wallinder I 2014 *In vitro* biocompatibility of CoCrMo dental alloys fabricated by selective laser melting *Dental Mater.* **30** 525–34
- [68] Vaithilingam J, Kilsby S, Goodridge R D, Christie S D R, Edmondson S and Hague R J M 2015 Functionalisation of Ti6Al4V components fabricated using selective laser melting with a bioactive compound *Mater. Sci. Eng.: C* **46** 52–61
- [69] Shirazi F S, Mehrali M, Ataollahi Oshkour A, Cornelis Metselaar H S, Kadri N A and Abu Osman N A 2013 Characterization and mechanical properties of calcium silicate/citric acid-based polymer composite materials *Int. J. Appl. Ceram. Technol.* **12** 371–6
- [70] Shor L, Güçeri S, Wen X, Gandhi M and Sun W 2007 Fabrication of three-dimensional polycaprolactone/hydroxyapatite tissue scaffolds and osteoblast-scaffold interactions *in vitro* *Biomaterials* **28** 5291–7
- [71] Eosoly S, Vrana N E, Lohfeld S, Hindie M and Looney L 2012 Interaction of cell culture with composition effects on the mechanical properties of polycaprolactone-hydroxyapatite scaffolds fabricated via selective laser sintering (SLS) *Mater. Sci. Eng.: C* **32** 2250–7
- [72] Chua C K, Leong K F, Tan K H, Wiria F E and Cheah C M 2004 Development of tissue scaffolds using selective laser sintering of polyvinyl alcohol/hydroxyapatite biocomposite for craniofacial and joint defects *J. Mater. Sci., Mater. Med.* **15** 1113–21

- [73] Bose S, Tarafder S, Banerjee S and Bandyopadhyay A 2011 *Biomaterials Science—Processing, Properties, and Applications* (New York: Wiley) pp 135–45
- [74] Ma R and Tang T 2014 Current strategies to improve the bioactivity of PEEK *Int. J. Mol. Sci.* **15** 5426–45
- [75] Puppi D, Chiellini F, Piras A M and Chiellini E 2010 Polymeric materials for bone and cartilage repair *Prog. Polym. Sci.* **35** 403–40
- [76] Han C-M, Lee E-J, Kim H-E, Koh Y-H, Kim K N, Ha Y and Kuh S-U 2010 The electron beam deposition of titanium on polyetheretherketone (PEEK) and the resulting enhanced biological properties *Biomaterials* **31** 3465–70
- [77] Shuai C, Li P, Liu J and Peng S 2013 Optimization of TCP/HAP ratio for better properties of calcium phosphate scaffold via selective laser sintering *Mater. Charact.* **77** 23–31
- [78] Shuai C, Feng P, Cao C and Peng S 2013 Processing and characterization of laser sintered hydroxyapatite scaffold for tissue engineering *Biotechnol. Bioprocess Eng.* **18** 520–7
- [79] Shuai C-J, Mao Z-Z, Han Z-K and Peng S-P 2014 Preparation of complex porous scaffolds via selective laser sintering of poly (vinyl alcohol)/calcium silicate *J. Bioact. Compat. Polym.: Biomed. Appl.* **29** 110–20
- [80] Feng P, Wei P, Li P, Gao C, Shuai C and Peng S 2014 Calcium silicate ceramic scaffolds toughened with hydroxyapatite whiskers for bone tissue engineering *Mater. Charact.* **97** 47–56
- [81] Mehrali M, Moghaddam E, Shirazi S F S, Baradaran S, Mehrali M, Latibari S T, Metselaar H S C, Kadri N A, Zandi K and Osman N A A 2014 Mechanical and *In Vitro* biological performance of graphene nanoplatelets reinforced calcium silicate composite *PLoS One* **9** e106802
- [82] Velez M, Jung S, Kolan K, Leu M, Day D and Chu T M 2011 *In vivo* evaluation of 13-93 bioactive glass scaffolds made by selective laser sintering (SLS) *Biomaterials Science: Processing, Properties and Applications II: Ceramic Transactions vol 237* pp 91–9
- [83] Shishkovsky I, Volova L, Kuznetsov M, Morozov Y G and Parkin I 2008 Porous biocompatible implants and tissue scaffolds synthesized by selective laser sintering from Ti and NiTi *J. Mater. Chem.* **18** 1309–17
- [84] Duan B and Wang M 2011 Selective laser sintering and its application in biomedical engineering *MRS Bull.* **36** 998–1005
- [85] Facchini L, Magalini E, Robotti P, Molinari A, Höges S and Wissenbach K 2010 Ductility of a Ti-6Al-4V alloy produced by selective laser melting of prealloyed powders *Rapid Prototyping J.* **16** 450–9
- [86] Vrancken B, Thijs L, Kruth J-P and Van Humbeeck J 2012 Heat treatment of Ti6Al4V produced by selective laser melting: microstructure and mechanical properties *J. Alloys Compd.* **541** 177–85
- [87] Zhang Y, Hao L, Savalani M, Harris R A, Di Silvio L and Tanner K 2009 *In vitro* biocompatibility of hydroxyapatite-reinforced polymeric composites manufactured by selective laser sintering *J. Biomed. Mater. Res.: A* **91** 1018–27
- [88] Chen C-H, Lee M-Y, Shyu V B-H, Chen Y-C, Chen C-T and Chen J-P 2014 Surface modification of polycaprolactone scaffolds fabricated via selective laser sintering for cartilage tissue engineering *Mater. Sci. Eng.: C* **40** 389–97
- [89] Chen C-H, Shyu V B-H, Chen J-P and Lee M-Y 2014 Selective laser sintered poly- ϵ -caprolactone scaffold hybridized with collagen hydrogel for cartilage tissue engineering *Biofabrication* **6** 015004
- [90] Liao H-T, Chang K-H, Jiang Y, Chen J-P and Lee M-Y 2011 Fabrication of tissue engineered PCL scaffold by selective laser-sintered machine for osteogenesis of adipose-derived stem cells: the research has proven that a bone tissue-engineered scaffold can be made using the selective laser sintering method *Virtual Phys. Prototyping* **6** 57–60
- [91] Das S, Hollister S J, Flanagan C, Adewunmi A, Bark K, Chen C, Ramaswamy K, Rose D and Widjaja E 2003 Freeform fabrication of Nylon-6 tissue engineering scaffolds *Rapid Prototyping J.* **9** 43–9
- [92] Lohfeld S, Cahill S, Barron V, McHugh P, Dürselen L, Kreja L, Bausewein C and Ignatius A 2012 Fabrication, mechanical and *in vivo* performance of polycaprolactone/tricalcium phosphate composite scaffolds *Acta Biomaterialia* **8** 3446–56
- [93] Saito E, Suarez-Gonzalez D, Murphy W L and Hollister S J 2014 Biomineral coating increases bone formation by ex vivo BMP-7 gene therapy in rapid prototyped poly (l-lactic acid)(PLLA) and poly (ϵ -caprolactone)(PCL) porous scaffolds *Adv. Healthc. Mater.* **4** 621–32
- [94] Sudarmadji N, Tan J, Leong K, Chua C and Loh Y 2011 Investigation of the mechanical properties and porosity relationships in selective laser-sintered polyhedral for functionally graded scaffolds *Acta Biomater.* **7** 530–7
- [95] Deng J, Li P, Gao C, Feng P, Shuai C and Peng S 2014 Bioactivity improvement of forsterite-based scaffolds with nano-58 S bioactive glass *Mater. Manuf. Process.* **29** 877–84
- [96] Kullmann C, Schirmer N C, Lee M-T, Ko S H, Hotz N, Grigoropoulos C P and Poulidakos D 2012 3D microstructures by piezoelectric inkjet printing of gold nanofluids *J. Micromech. Microeng.* **22** 055022
- [97] Kumar A V, Dutta A and Fay J E 2004 Electrophotographic printing of part and binder powders *Rapid Prototyping J.* **10** 7–13
- [98] Noguera R, Lejeune M and Chartier T 2005 3D fine scale ceramic components formed by ink-jet prototyping process *J. Eur. Ceram. Soc.* **25** 2055–9
- [99] Saijo H, Igawa K, Kanno Y, Mori Y, Kondo K, Shimizu K, Suzuki S, Chikazu D, Iino M and Anzai M 2009 Maxillofacial reconstruction using custom-made artificial bones fabricated by inkjet printing technology *J. Artif. Organs* **12** 200–5
- [100] Farzadi A, Solati-Hashjin M, Asadi-Eydivand M and Osman N A A 2014 Effect of layer thickness and printing orientation on mechanical properties and dimensional accuracy of 3D printed porous samples for bone tissue engineering *PLoS One* **9** e108252
- [101] Murphy S V and Atala A 2014 3D bioprinting of tissues and organs *Nat. Biotechnol.* **32** 773–85
- [102] Rahmati S, Shirazi S and Baghayeri H 2009 Piezo-electric head application in a new 3D printing design *Rapid Prototyping J.* **15** 187–91
- [103] Xu T, Jin J, Gregory C, Hickman J J and Boland T 2005 Inkjet printing of viable mammalian cells *Biomaterials* **26** 93–9
- [104] Kim J D, Choi J S, Kim B S, Choi Y C and Cho Y W 2010 Piezoelectric inkjet printing of polymers: stem cell patterning on polymer substrates *Polymer* **51** 2147–54
- [105] Calvert P 2001 Inkjet printing for materials and devices *Chem. Mat.* **13** 3299–305
- [106] Wood V, Panzer M J, Chen J, Bradley M S, Halpert J E, Bawendi M G and Bulović V 2009 Inkjet-printed quantum dot-polymer composites for full-color ac-driven displays *Adv. Mater.* **21** 2151–5
- [107] Rahmati S, Shirazi F and Baghayeri H 2009 Perusing piezoelectric head performance in a new 3-D printing design *Tsinghua Sci. Technol.* **14** (Suppl. 1) 24–8
- [108] Peters F, Groisman D, Davids R, Hänel T, Dürr H and Klein M 2006 Comparative study of patient individual implants from β -tricalcium phosphate made by different techniques based on CT data *Mater.wiss. Werkst.tech.* **37** 457–61

- [109] Castilho M, Moseke C, Ewald A, Gbureck U, Groll J, Pires I, Teßmar J and Vorndran E 2014 Direct 3D powder printing of biphasic calcium phosphate scaffolds for substitution of complex bone defects *Biofabrication* **6** 015006
- [110] Wu C, Fan W, Zhou Y, Luo Y, Gelinsky M, Chang J and Xiao Y 2012 3D-printing of highly uniform CaSiO₃ ceramic scaffolds: preparation, characterization and *in vivo* osteogenesis *J. Mater. Chem.* **22** 12288–95
- [111] Vorndran E, Klarner M, Klammert U, Grover L M, Patel S, Barralet J E and Gbureck U 2008 3D powder printing of β -tricalcium phosphate ceramics using different strategies *Adv. Eng. Mater.* **10** B67–71
- [112] Xu T, Binder K W, Albanna M Z, Dice D, Zhao W, Yoo J J and Atala A 2013 Hybrid printing of mechanically and biologically improved constructs for cartilage tissue engineering applications *Biofabrication* **5** 015001
- [113] Lanzetta M and Sachs E 2003 Improved surface finish in 3D printing using bimodal powder distribution *Rapid Prototyping J.* **9** 157–66
- [114] Derby B 2011 Inkjet printing ceramics: from drops to solid *J. Eur. Ceram. Soc.* **31** 2543–50
- [115] Hogekamp S and Pohl M 2004 Methods for characterizing wetting and dispersing of powder *Chem. Ing. Tech.* **76** 385–90
- [116] Hapgood K P, Litster J D, Biggs S R and Howes T 2002 Drop penetration into porous powder beds *J. Colloid Interface Sci.* **253** 353–66
- [117] Giordano R A, Wu B M, Borland S W, Cima L G, Sachs E M and Cima M J 1996 Mechanical properties of dense polylactic acid structures fabricated by three dimensional printing *J. Biomater. Sci.—Polym. Ed.* **8** 63–75
- [118] Bohner M 2000 Calcium orthophosphates in medicine: from ceramics to calcium phosphate cements *Injury-Int. J. Care Inj.* **31** S37–47
- [119] Bohner M, Gbureck U and Barralet J E 2005 Technological issues for the development of more efficient calcium phosphate bone cements: a critical assessment *Biomaterials* **26** 6423–9
- [120] Fielding G A, Bandyopadhyay A and Bose S 2012 Effects of silica and zinc oxide doping on mechanical and biological properties of 3D *Dental Mater.* **28** 113–22
- [121] Butscher A, Bohner M, Roth C, Ernstberger A, Heuberger R, Doebelin N, Rudolf von Rohr P and Müller R 2012 Printability of calcium phosphate powders for three-dimensional printing of tissue engineering scaffolds *Acta Biomater.* **8** 373–85
- [122] Irsen S H, Leukers B, Hockling C, Tille C and Seitz H 2006 Bioceramic granulates for use in 3D printing: process engineering aspects *Mater.wiss. Werkst.tech.* **37** 533–7
- [123] Seitz H, Rieder W, Irsen S, Leukers B and Tille C 2005 Three-dimensional printing of porous ceramic scaffolds for bone tissue engineering *J. Biomed. Mater. Res. B* **74B** 782–8
- [124] Butscher A, Bohner M, Hofmann S, Gauckler L and Muller R 2011 Structural and material approaches to bone tissue engineering in powder-based three-dimensional printing *Acta Biomater.* **7** 907–20
- [125] Mourino V and Boccaccini A R 2010 Bone tissue engineering therapeutics: controlled drug delivery in three-dimensional scaffolds *J. R. Soc. Interface* **7** 209–27
- [126] Suwanprateeb J, Kerdsook S, Boonsiri T and Pratumpong P 2011 Evaluation of heat treatment regimes and their influences on the properties of powder-printed high-density polyethylene bone implant *Polym. Int.* **60** 758–64
- [127] Suwanprateeb J and Chumnanklang R 2006 Three-dimensional printing of porous polyethylene structure using water-based binders *J. Biomed. Mater. Res.: B Appl. Biomater.* **78B** 138–45
- [128] Lam C X F, Mo X M, Teoh S H and Hutmacher D W 2002 Scaffold development using 3D printing with a starch-based polymer *Mater. Sci. Eng.: C* **20** 49–56
- [129] Gbureck U, Hölzel T, Doillon C J, Mueller F A and Barralet J E 2007 Direct printing of bioceramic implants with spatially localized angiogenic factors *Adv. Mater.* **19** 795–800
- [130] Yang S, Leong K-F, Du Z and Chua C-K 2002 The design of scaffolds for use in tissue engineering: II. Rapid prototyping techniques *Tissue Eng.* **8** 1–11
- [131] Igawa K et al 2006 Tailor-made tricalcium phosphate bone implant directly fabricated by a three-dimensional ink-jet printer *J. Artif. Organs* **9** 234–40
- [132] Inzana J A, Olvera D, Fuller S M, Kelly J P, Graeve O A, Schwarz E M, Kates S L and Awad H A 2014 3D printing of composite calcium phosphate and collagen scaffolds for bone regeneration *Biomaterials* **35** 4026–34
- [133] Zhou Z, Buchanan F, Mitchell C and Dunne N 2014 Printability of calcium phosphate: calcium sulfate powders for the application of tissue engineered bone scaffolds using the 3D printing technique *Mater. Sci. Eng.: C* **38** 1–10
- [134] Fierz F C, Beckmann F, Huser M, Irsen S H, Leukers B, Witte F, Degistirici Ö, Andronache A, Thie M and Müller B 2008 The morphology of anisotropic 3D-printed hydroxyapatite scaffolds *Biomaterials* **29** 3799–806
- [135] Tarafder S, Balla V K, Davies N M, Bandyopadhyay A and Bose S 2013 Microwave-sintered 3D printed tricalcium phosphate scaffolds for bone tissue engineering *J. Tissue Eng. Regenerative Med.* **7** 631–41
- [136] Zhang J, Zhao S, Zhu Y, Huang Y, Zhu M, Tao C and Zhang C 2014 Three-dimensional printing of strontium-containing mesoporous bioactive glass scaffolds for bone regeneration *Acta Biomater.* **10** 2269–81
- [137] Wu C, Ramaswamy Y, Boughton P and Zreiqat H 2008 Improvement of mechanical and biological properties of porous CaSiO₃ scaffolds by poly(d,l-lactic acid) modification *Acta Biomater.* **4** 343–53
- [138] Cox S C, Thornby J A, Gibbons G J, Williams M A and Mallick K K 2015 3D printing of porous hydroxyapatite scaffolds intended for use in bone tissue engineering applications *Mater. Sci. Eng.: C* **47** 237–47
- [139] Shirazi F, Mehrali M, Oshkour A, Metselaar H, Kadri N and Abu Osman N 2014 Mechanical and physical properties of calcium silicate/alumina composite for biomedical engineering applications *J. Mech. Behav. Biomed. Mater.* **30** 168–75
- [140] Wang J W and Shaw L L 2006 Fabrication of functionally graded materials via inkjet color printing *J. Am. Ceram. Soc.* **89** 3285–9
- [141] Becker S T, Douglas T, Acil Y, Seitz H, Sivananthan S, Wiltfang J and Warnke P H 2010 Biocompatibility of individually designed scaffolds with human periosteum for use in tissue engineering *J. Mater. Sci., Mater. Med.* **21** 1255–62
- [142] Hashizume M and Yamaguchi M 1994 Effect of beta-alanyl-l-histidinato zinc on differentiation of osteoblastic mc3t3-e1 cells—increases in alkaline-phosphatase activity and protein-concentration *Mol. Cell. Biochem.* **131** 19–24
- [143] Yamaguchi M and Yamaguchi R 1986 Action of zinc on bone metabolism in rats—increases in alkaline-phosphatase activity and dna content *Biochem. Pharmacol.* **35** 773–7
- [144] Gbureck U, Hölzel T, Doillon C J, Müller F A and Barralet J E 2007 Direct printing of bioceramic implants with spatially localized angiogenic factors *Adv. Mater.* **19** 795–800

- [145] Tarafder S, Davies N M, Bandyopadhyay A and Bose S 2013 3D printed tricalcium phosphate bone tissue engineering scaffolds: effect of SrO and MgO doping on *in vivo* osteogenesis in a rat distal femoral defect model *Biomater. Sci.* **1** 1250–9
- [146] Bose S, Vahabzadeh S and Bandyopadhyay A 2013 Bone tissue engineering using 3D printing *Mater. Today* **16** 496–504
- [147] Traini T, Mangano C, Sammons R, Mangano F, Macchi A and Piattelli A 2008 Direct laser metal sintering as a new approach to fabrication of an isoelastic functionally graded material for manufacture of porous titanium dental implants *Dental Mater.* **24** 1525–33
- [148] Mangano F, Bazzoli M, Tettamanti L, Farronato D, Maineri M, Macchi A and Mangano C 2013 Custom-made, selective laser sintering (SLS) blade implants as a non-conventional solution for the prosthetic rehabilitation of extremely atrophied posterior mandible *Lasers Med. Sci.* **28** 1241–7